RESEARCH ARTICLE | MARCH 17 2025

What does an ion feel at the electrochemical interface? Revisiting electrosorption through nonlocal electrostatics

Special Collection: Festschrift for Abraham Nitzan

Jonathan G. Hedley ; Kavin K. Bhatt ; Hélène Berthoumieux ; Alexei A. Kornyshev

J. Chem. Phys. 162, 114703 (2025)
https://doi.org/10.1063/5.0254033

The Journal of Chemical Physics ARTICLE pubs.aip.org/aip/jcp

What does an ion feel at the electrochemical interface? Revisiting electrosorption through nonlocal electrostatics

Cite as: J. Chem. Phys. 162, 114703 (2025); doi: 10.1063/5.0254033
Submitted: 20 December 2024 • Accepted: 18 February 2025 •
Published Online: 17 March 2025

Jonathan G. Hedley,[1,2,a] Kavin K. Bhatt,[1] Hélène Berthoumieux,[3] and Alexei A. Kornyshev[1,4,b]

AFFILIATIONS

[1] Department of Chemistry, Imperial College London, Molecular Sciences Research Hub, London W12 0BZ, United Kingdom
[2] Department of Engineering Science, University of Oxford, Oxford OX1 3QD, United Kingdom
[3] UMR CNRS Gulliver 7083, ESPCI–PSL Research University, 75005 Paris, France
[4] Thomas Young Centre for Theory and Simulation of Materials, Imperial College London, South Kensington Campus, London SW7 2AZ, United Kingdom

Note: This paper is part of the JCP Special Topic, Festschrift for Abraham Nitzan.
[a] jonathan.hedley@eng.ox.ac.uk
[b] **Author to whom correspondence should be addressed:** a.kornyshev@imperial.ac.uk

ABSTRACT

The traditional Gouy–Chapman–Stern theory has been effective in explaining the behavior of dilute electrolytes in the electrical double layer but falls short when it comes to describing how ions behave at the metal/electrolyte interface. This is because it overlooks key factors such as the molecular structure of water at the interface and the effects of electron screening in the metal. To address these gaps, we revisit ion adsorption at the metal/electrolyte interface. The approach combines the method of images with a field-theoretic framework for dilute electrolytes and metals described by the Thomas–Fermi model. Nonlocal polarization correlations in water are described by a first-order gradient expansion in the Landau free energy functional. Unlike earlier approaches that relied on the "specular reflection approximation," our method provides a less constrained way to handle the complex electrostatic boundary conditions at the interface. Analyzing the behavior of a test charge near the interface, an electrostatic energy minimum is found. This minimum depends on the metal's screening properties and the overall potential drop across the double layer. In addition, the alignment of water dipoles at the interface creates an asymmetry in the energy experienced by positively and negatively charged ions. Finally, we derived an expression for the electrosorption isotherm by describing both the distribution of the electrostatic potential and the lateral interactions between charges along the interface. Our findings highlight how the structure of interfacial water can drive processes such as underpotential deposition by creating favorable electrostatic conditions for ion adsorption.

I. INTRODUCTION

A question that arises frequently in the fields of soft matter and electrochemistry is the following: "What do ions actually feel at a charged interface?" Such an apparently simple question is fundamental to a multitude of applications. In biology, spontaneously charged low dielectric/aqueous electrolyte interfaces frequently appear, for example, in proteins, lipid bilayers, and chromosomes. Understanding what ions may experience at those interfaces can lead to a more detailed picture of the double layer and, consequently, how the forces and interactions of these biological interfaces are determined. In electrochemistry, one of the most frequent interfaces encountered is the polarizable metal electrode–aqueous electrolyte interface. With the coupled screening effects of both metal electrons and electrolyte ions, and also the polar solvent, playing prominent roles in determining the electric field near the interface, clearly, one cannot overstate the complexity of what initially appears to be a simple and straightforward question.

Of course, this is not a recent question, having been initially tackled through the guise of the "electrical double layer" by Helmholtz in 1853,[1,2] followed by Gouy, Chapman, and Stern in the 20th century.[3–5] However, since those seminal works, simulation[6–11] and theoretical (for reviews, see, e.g., Refs. 12 and 13) studies have shown the picture of the double layer and the distribution of ions from a charged interface to be much different, with water structure playing a markedly important role close to the interface. This water structure has been shown to lead to oscillatory "overscreening" patterns in the electrostatic potential distribution, which has been theorized to lead to the layered packing of ions with alternating sign normal to the interface,[14] a dramatically different picture from that of Gouy–Chapman–Stern theory. The notion that ions feel and arrange themselves according to this oscillating electric field due to water structure sounds almost incredible and is being debated within the scientific community,[15] although many experimental measurements using atomic force microscopy appear to support this picture.[16–20] However, obviously, correlations in the ion subsystem would overwhelm their distribution above some critical concentrations of electrolyte so that they may form their own structures, affected but not fully dominated by the solvent molecular correlations. This feature was well studied in theories based on the primitive, structureless model of the solvent (its description solely by a macroscopic dielectric constant), known as the Kirkwood transition. How a similar effect could take place accounting for the molecular structure of water is yet not known. It has not been theoretically described so far, neither in the bulk nor in the electrical double layer.

When considering what a single ion feels, a slightly different approach is required than those above.[21–23] Here, we revisit the classical problem of image charges. Well studied in most undergraduate electrostatics courses, the *method of images* is used to calculate the electrostatics of charges at interfaces. Whether the interface consists of two dielectrics or a dielectric and a conductor, such an approach can predict if an ion is either attracted to or repelled from the interface in question, based purely on the macroscopic dielectric constants of the contacting media.[24] Of course, this classical macroscopic picture fails to account for any molecular structure in the contacting media. A natural approach to introduce this structure is through *nonlocal electrostatics*, by means of generalizing the dielectric constant to the nonlocal dielectric function, $\varepsilon(\mathbf{r},\mathbf{r}')$, or more usually its wavenumber-dependent Fourier transform, $\varepsilon(\mathbf{k})$.[25] Local, macroscopic theory formulations for the method of images obviously then break down for contacting nonlocal media. This, however, has not stopped attempts to understand how nonlocality may affect charges at interfaces. A first attempt by Inkson showed for the first time how attractive and repulsive branches of the self-energy of a point charge at a semiconductor junction could lead to significant variations from the classical laws.[26] The problem was later investigated again by Kornyshev *et al.* in the context of electrochemical interfaces for the interface between a Thomas–Fermi (TF) metal and a dielectric, representing water.[21] Soon after, this was generalized for the interface between two nonlocal media[22,23,27] using the specular reflection approximation (SRA),[28] which was utilized in many follow-up works, particularly by Gabovich *et al.*[29–34] However, this SRA appears to fail when the overscreening dielectric response of the dielectric medium is accounted for (see Sec. II B 2 below).

Of course, one may ask whether simulations have been able to validate these theoretical models proposed above. Indeed, the classical molecular dynamics method does not generally allow the inclusion of these "quantum" effects at metallic interfaces, although strategies to capture the screening effects in metals have more recently been developed.[35–42] Also recently developed is the surface response function approach.[43–45] This elegant theoretical method provides a formal expression for the dielectric response of nonlocal interfacial systems, including complex media such as water or graphene. While no *a priori* assumptions are required in the formulation, in practice the surface response function is evaluated using approximations such as the SRA or by using inputs from molecular dynamics simulations.

In this paper, this rich history is built upon, revisiting again the problem of the Thomas–Fermi metal–nonlocal water interface. While the topic of oscillations in water will not be developed in this theory here, the method presented lays the groundwork for the inclusion of such a complicated effect, which currently no theory to our knowledge is able to fully account for. Thus, the results here are obtained purely in the context of the so-called Lorentzian dielectric function,[46] almost as a *proof of concept*. Furthermore, only the physical phenomenon of ion adsorption is considered here, and so here the interest will be on how, from purely electrostatic considerations, an ion may approach the interface.

To begin, a brief introduction to the classical theory is provided in Sec. II A, not only to give context to the method of images but also as a reference to which the developed theory can be compared. Next, in Sec. II B, preliminary results are obtained for the Thomas–Fermi metal–Lorentzian water interface, using a general formulation of this problem based on the SRA,[22] detailing its limitations. Then, the new approach, based on a field theoretical (FT) free energy functional, is detailed in Sec. III. Defining the bulk free energy functional on both sides of the interface, constitutive equations can be obtained without specifying any explicit form of the dielectric function or introducing any approximations for the dielectric function at the interface. These approaches, however, all assume that the only contribution to the electric field arises from the test ion itself; this is clearly not the case in reality, where the double layer generated by an external electrode potential, or by chemisorbed water at the interface, can influence the test charge. These effects are accounted for in Sec. IV. With all this taken into account, the full electrostatic potential distribution is calculated in Sec. V, showing the penetration of the ion field into the metal, providing further context to the results described earlier in this paper. The lateral interaction of charges in the plane of the surface is also studied, an important contribution to the final section of the paper, Sec. VI, where an adsorption isotherm model (utilizing the cut-out disk approximation[47]) is developed, showing how the model parameters and physical effects can manifest in these experimentally measurable profiles. Note that Gaussian units are used throughout this paper.

II. THE METHOD OF IMAGES: A BRIEF OVERVIEW

A. Classical electrostatic approach

Let us consider a point charge, in a dielectric (I) at $z = a$ above an uncharged semi-infinite metal plate (II) at $z = 0$ [see Fig. 1(a)]. If the metal is a perfect conductor, that is, its dielectric constant $\varepsilon_{II} = \infty$, then the electric field inside the metal is zero. To ensure that

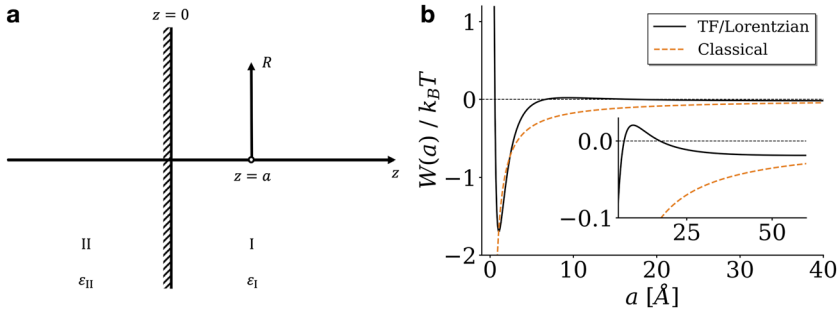

FIG. 1. Self-energy of a point charge at the metal–water interface within the SRA. Panel (a) shows a physical representation of the system at hand, and panel (b) plots the self-energy profile as calculated from Eq. (14), showing an adsorption minimum close to the interface. Here, the parameters for the Thomas–Fermi metal are $\varepsilon_M = 2$ and $\varkappa_{TF} = 2$ Å^{-1} and the parameters for the Lorentzian water are $\varepsilon = 80$, $\varepsilon_* = 5$, and $\Lambda = 3$ Å. The inset shows the long-range behavior, with a small repulsive barrier. The classical self-energy law, Eq. (7), is plotted for reference in orange.

this is still the case when the point charge approaches the metal plate, a surface charge density that exactly opposes the point charge is induced such that the field produced by the point charge is perfectly screened at the interface.

This, however, does not tell us how to calculate the electrostatic potential in all space. Conveniently, a nifty trick is employed here; if the plate is uncharged, the electric field is zero at the interface, and the field then becomes equivalent to that of a dipole, which can be simulated by placing an image of the charge with equal and opposite magnitude at $z = -a$. With this, the total field at the interface can be computed with relative ease.

Of course, just the metal–dielectric interface was considered above, but the method of images can be adopted for any interface between two contacting media. For a point charge above a dielectric–dielectric interface, the "image" charge will be of a different magnitude, potentially even of the same sign as the test charge, if $\varepsilon_1 > \varepsilon_2$.[48]

Therefore, while later in this paper the theory will generally be applied in the context of the metal–water interface, the classical approach to a charge at an interface presented here will be generalized for the dielectric–dielectric interface, from which the limiting case of a metal–water interface can be investigated.

1. Electrostatic potential and local boundary conditions

To understand how the method of images works here, let us begin by revisiting the classical picture of an interface of two dielectrics, each characterized by macroscopic dielectric constants.[24,48] The system will be setup as such: consider two half-spaces, medium I ($z > 0$) with dielectric constant ε_I and medium II ($z < 0$) with dielectric constant ε_{II}. A point charge, with charge q, is placed at $z = a$. Its images, q' and q'', are placed in medium I at $z = a$ and in medium II at $z = -a$, respectively. The electrostatic potential in all space can then be written as[48]

$$\varphi(\mathbf{r}) = \begin{cases} \frac{1}{\varepsilon_I}\left(\frac{q}{R_-} + \frac{q'}{R_+}\right), & z > 0, \\ \frac{1}{\varepsilon_{II}}\left(\frac{q''}{R_-}\right), & z < 0, \end{cases} \tag{1}$$

where $R_\pm = \sqrt{R^2 + (z \pm a)^2}$, thus defining a cylindrical coordinate system, which is convenient for the problem. However, in writing this, it is not clear what the magnitudes of q' and q'' are in terms of q. To find these, the boundary conditions must be defined.

The Maxwell boundary conditions for electric fields can be derived from Faraday's and Gauss's laws of electromagnetism, stating that, at $z = 0$,

1. The tangential component of the electric field across the interface is continuous, $\hat{\mathbf{n}} \times (\mathbf{E}_I - \mathbf{E}_{II}) = 0$, where $\hat{\mathbf{n}}$ is the normal vector from medium II to I.
2. The normal component of the displacement field across the interface equals the surface charge density, $\hat{\mathbf{n}} \cdot (\mathbf{D}_I - \mathbf{D}_{II}) = 4\pi\tilde{\sigma}$. Here, however, $\tilde{\sigma} = 0$, and the displacement field is, therefore, continuous over the interface.

Within the limit of local electrostatics, these boundary conditions can be related reasonably easily to Eq. (1). The electrostatic potential is related to the electric field by $\mathbf{E} = -\nabla\varphi$, so the tangential component is simply given by $\mathbf{E}_\parallel = -\partial_R\varphi(z, R)$. In addition, the displacement field in a medium i is given by $\mathbf{D}_i = \varepsilon_i\mathbf{E}_i$, and so by the same relationship of electrostatic potential to the electric field, the normal component of the displacement field is given by $\mathbf{D}_{\perp,i} = -\varepsilon_i\partial_z\varphi_i(R, z)$. Thus, these boundary conditions yield the following solutions for q' and q'':

$$q' = \frac{\varepsilon_I - \varepsilon_{II}}{\varepsilon_I + \varepsilon_{II}} \cdot q, \tag{2}$$

$$q'' = \frac{2\varepsilon_{II}}{\varepsilon_I + \varepsilon_{II}} \cdot q, \tag{3}$$

which can be inserted into Eq. (1) to give the solution for the potential in all space,

$$\varphi(\mathbf{r}) = \begin{cases} \frac{q}{\varepsilon_I}\left(\frac{1}{R_-} + \frac{1}{R_+} \cdot \frac{\varepsilon_I - \varepsilon_{II}}{\varepsilon_I + \varepsilon_{II}}\right), & z > 0, \\ \frac{2q}{\varepsilon_I + \varepsilon_{II}}\left(\frac{1}{R_-}\right), & z < 0. \end{cases} \tag{4}$$

Examining this result, an interesting conclusion can be made; depending on the dielectric constants of the two contacting media,

the electrostatic potential can either be enhanced or reduced in medium I. In the case of a metal, $\varepsilon_{II} \to \infty$ and the solution for $z > 0$ clearly becomes that of a dipole centered around $z = 0$.

However, calculating the electrostatic potential does not yet provide any information on what the point charge may feel as it approaches the interface. To do this, the self-energy of the charge should be calculated.

2. Self-energy of a point charge

The self-energy, W, of a point charge at the interface, also known as the "image potential," is defined as the energy of bringing a charge from a homogeneous medium to the interface. This self-energy can then be calculated by making use of the Güntelberg charging equation,

$$W(a) = \lim_{\substack{z\to a \\ R\to 0}} \int_0^q dq[\varphi(z,R) - \varphi^{(0)}(z,R)], \tag{5}$$

where $\varphi^{(0)}$ is the potential created by the point charge in the bulk of the medium it is placed in. In the limit of local electrostatics, this is simply given by the Coulomb potential, $\varphi^{(0)}(\mathbf{r}) = q/\varepsilon_I r$, where $r = |\mathbf{r}|$. Thus, plugging Eq. (4) into (5), a rather simple law for the self-energy is obtained,

$$W(a) = \frac{q^2}{4\varepsilon_I a}\left(\frac{\varepsilon_I - \varepsilon_{II}}{\varepsilon_I + \varepsilon_{II}}\right). \tag{6}$$

Such a simple expression yields great consequences; as done before for the potential, consider how changing the values of ε_I and ε_{II} may influence the self-energy. If $\varepsilon_I - \varepsilon_{II} > 0$, then the self-energy is positive, and the charge is repelled from the interface. Conversely, if $\varepsilon_I - \varepsilon_{II} < 0$, then the self-energy is negative, and the charge is attracted to the interface. This intuitively makes sense; the point charge wants to be in a medium where its field is screened more strongly and so will want to reside wherever the dielectric constant is higher.

Considering this expression specifically for the metal–water interface, taking the limit as $\varepsilon_{II} \to \infty$ and $\varepsilon_I \to \varepsilon$,

$$W(a) = -\frac{q^2}{4\varepsilon a}, \tag{7}$$

stating that the charge will always be attracted to the interface by a simple inverse-distance law.

The analysis drawn above is all known from textbooks,[24,48] but we have reproduced it for comparison with the results that the nonlocal electrostatic and field theories would deliver, as presented below.

B. An initial nonlocal electrostatic approach

It is possible to generalize this classical theory to two contacting nonlocal media in the context of the factor in Eq. (6). One can write a crude interpolation formula, reproducing the classical result in the case of "large" a and the short-range behavior in the limit of "small" a.[46] This reads

$$W(a) \approx \frac{q^2}{4a\varepsilon_I(k = a^{-1})}\left(\frac{\varepsilon_I(k = a^{-1}) - \varepsilon_{II}(k = a^{-1})}{\varepsilon_I(k = a^{-1}) + \varepsilon_{II}(k = a^{-1})}\right), \tag{8}$$

where $k = |\mathbf{k}|$. While such an expression is in no way rigorously justified, it at least gives an insight into what one may expect at a nonlocal–nonlocal interface. Depending on the interplay of the dielectric functions of the two contacting media, $\varepsilon_I(k)$ and $\varepsilon_{II}(k)$, one may expect to see regions of both attraction and repulsion from the interface, potentially resulting in some kind of physical electrostatic minimum close to the interface. To rigorously examine such a behavior, let us instead attempt to approximate the nonlocal–nonlocal interface and derive the self-energy within that approximation.

1. Self-energy within the specular reflection approximation

While the method of images within a classical picture of electrostatics is relatively straightforward, the same cannot be said when generalizing for a nonlocal case. The reason for this lies in the boundary conditions; when the translational symmetry of the system in the z-axis is broken at the interface, it is no longer possible to describe the medium by some homogeneous and isotropic $\varepsilon(|\mathbf{r} - \mathbf{r}'|)$. Instead, one must write $\varepsilon(z, z'; \mathbf{R})$ to account for this, the form of which is not particularly clear. In addition, it is no longer possible to write the local formulation of the second Maxwell boundary condition on the displacement field, $\mathbf{D}$, as in Sec. II A. Instead, the displacement field at the interface in medium I becomes

$$\mathbf{D}_I(z = 0) \cdot \hat{\mathbf{n}} = -\int_0^\infty dz' \varepsilon_{I,zz}(z = 0, z'; \mathbf{R}) \frac{\partial \varphi}{\partial z'}, \tag{9}$$

with a similar expression for medium II,[22,46,49] thus defining a set of highly nontrivial integro-differential equations to solve for the system, made even more complicated by the unclear form of the dielectric function.

To make any progress with such an expression, some approximations must be made. The most popular of these was the *Specular Reflection Approximation* (SRA),[28] which approximates the dielectric function at the interface as

$$\begin{aligned} \varepsilon_{zz}(z, z'; \mathbf{R}) &= \varepsilon_{zz}^{(j)}(z - z'; \mathbf{R}) - \varepsilon_{zz}^{(j)}(z + z'; \mathbf{R}), \\ \varepsilon_{\alpha\alpha}(z, z'; \mathbf{R}) &= \varepsilon_{\alpha\alpha}^{(j)}(z - z'; \mathbf{R}) + \varepsilon_{\alpha\alpha}^{(j)}(z + z'; \mathbf{R}), \end{aligned} \tag{10}$$

where $\alpha = x, y$, $j = I$ for $z, z' > 0$, and $j = II$ for $z, z' < 0$, and in all remaining cases, i.e., $z > 0$, $z' < 0$, and vice versa, $\varepsilon_{\alpha\beta}(z, z'; \mathbf{R}) = 0$. Such an approximation comes from the field of plasma physics and states that the polarization waves induced by the charge are perfectly reflected by the interface. By expressing the dielectric function at the interface as a combination of the dielectric functions in the bulk, it is possible to take the Fourier transforms of these expressions, which, when combined with the constitutive equation of nonlocal electrostatics,[46] yields, for a point charge placed at $z = a$ above an interface of two nonlocal media described by bulk dielectric functions $\varepsilon_I(k)$ and $\varepsilon_{II}(k)$, the electrostatic potential given by[22]

$$\varphi(z, R; a) = \int_0^\infty K dK J_0(KR) \tilde{\varphi}(z, K; a), \tag{11}$$

where K is the radial wavevector, $J_0(x)$ is the zeroth order Bessel function of the first kind,

$$\tilde{\varphi}(z,K;a) = \begin{cases} L_{\mathrm{I}}(z-a,K) + L_{\mathrm{I}}(z+a,K) - \dfrac{2L_{\mathrm{I}}(a,K)L_{\mathrm{I}}(z,K)}{L_{\mathrm{I}}(0,K)+L_{\mathrm{II}}(0,K)}, & z>0, \\ \dfrac{2L_{\mathrm{I}}(a,K)L_{\mathrm{II}}(z,K)}{L_{\mathrm{I}}(0,K)+L_{\mathrm{II}}(0,K)}, & z<0, \end{cases} \tag{12}$$

is the Fourier–Bessel transform of the electrostatic potential, and

$$L_{(j)}(z,K) = \frac{2}{\pi}\int_0^\infty dk_z \frac{\cos(k_z z)}{(k_z^2+K^2)\varepsilon_{(j)}\left(\sqrt{k_z^2+K^2}\right)}, \tag{13}$$

where $j = \mathrm{I}, \mathrm{II}$. For now, let us only consider the self-energy of the point charge within this formalism. Inserting Eqs. (11)–(13) into Eq. (5) yields

$$W(a) = \frac{q^2}{2}\int_0^\infty KdK\left\{L_{\mathrm{I}}(2a,K) - \frac{2[L_{\mathrm{I}}(a,K)]^2}{L_{\mathrm{I}}(0,K)+L_{\mathrm{II}}(0,K)}\right\}, \tag{14}$$

and so the problem is conveniently reduced to defining the dielectric functions of the two contacting media and calculating the integrals in Eqs. (13) and (14). While the exact derivation of this expression is not presented here, it can be found in Ref. 22, where it was first derived in 1980.

2. Approximating the Thomas–Fermi metal–nonlocal water interface

Now that a general expression for the self-energy of a point charge has been obtained, all that is left to do is to specify the dielectric functions of the two contacting media. This, however, is not always an easy task, but to see what may come out of it, let us consider some approximations. Considering medium I, the nonlocal dielectric response of water will be modeled by the Lorentzian dielectric function,

$$\varepsilon_{\mathrm{I}}(k) = \varepsilon_* + \frac{\varepsilon-\varepsilon_*}{1+\gamma\Lambda^2k^2}, \tag{15}$$

where $\gamma = \varepsilon/\varepsilon_*$. Such a model interpolates between a bulk dielectric constant, ε, at long distances $(k\to 0)$ and a short-range (high-frequency) dielectric constant, ε_*, at short distances $(k\to\infty)$, over some characteristic range, Λ. For water, the value of ε_* is estimated to be in the range of ~3–5.[46] Note that the local limit of such a dielectric function is obtained for $\varepsilon_* \to \varepsilon$, and thus $\gamma\to 1$, or $\Lambda\to 0$ Å. It is important here to warn straightaway that such an approximation does not do well in the domain of higher k-values, as it does not take into account the effect of overscreening in water.[50,51] For situations when such an approximation can still be applicable, see Ref. 14.

Moving to medium II, the simplest form the dielectric function can take is that of the *Thomas–Fermi* (TF) screening model. Such a model states that the dielectric function is given by

$$\varepsilon_{\mathrm{II}}(k) = \varepsilon_{\mathrm{M}}\left(1+\frac{\varkappa_{\mathrm{TF}}^2}{k^2}\right), \tag{16}$$

where $\varkappa_{\mathrm{TF}}^{-1}$ is the TF length, which is similar to the Debye length in that it describes the characteristic screening of a charge by the mobile electron cloud in the metal, and ε_{M} is the background permittivity of the metal atom skeleton. Examining the limiting behavior, the model also interpolates between the short-range behavior, $\varepsilon(k\to\infty)\to\varepsilon_{\mathrm{M}}$, and the long range behavior, $\varepsilon_{\mathrm{II}}(k\to 0)\to\infty$, which means that at long distances, the charge is perfectly screened within the metal. Such a model is also useful for investigating limiting cases; (i) for $\varkappa_{\mathrm{TF}}\to 0$, medium II acts as a dielectric with dielectric constant $\varepsilon_{\mathrm{II}} = \varepsilon_{\mathrm{M}}$, and (ii) for $\varkappa_{\mathrm{TF}}\to\infty$ and $\varepsilon_{\mathrm{M}}\to\infty$, medium II behaves as a classical metal. Note that the expression in Eq. (16) is again a linear approximation to the response in the metal and is thus applicable for weak electrode polarization. The TF screening model is, in fact, a simplification of the more general *Lindhard* model of screening; they coincide in the small-k limit.[52] As such, the TF model cannot describe Friedel oscillations, the effect of which can, however, be neglected as long as the test charge does not sit too close to the interface.[22]

Plugging Eqs. (15) and (16) into Eq. (13) yields the following solutions to the integrals, which can easily be obtained by contour integration:

$$L_{\mathrm{I}}(z,K) = \frac{1}{\varepsilon}\left[\frac{e^{-Kz}}{K} + (\gamma-1)\frac{e^{-z\sqrt{K^2+1/\Lambda^2}}}{\sqrt{K^2+1/\Lambda^2}}\right], \tag{17}$$

$$L_{\mathrm{II}}(z,K) = \frac{1}{\varepsilon_{\mathrm{M}}\sqrt{K^2+\varkappa_{\mathrm{TF}}^2}}e^{-z\sqrt{K^2+\varkappa_{\mathrm{TF}}^2}}, \tag{18}$$

both of which can be plugged directly into Eq. (14) to yield solutions for the self-energy. Importantly, it can be seen that taking the limiting cases described above for the dielectric functions, the classical laws for the self-energy in Eqs. (6) and (7) are obtained. Otherwise, the integral over K in Eq. (14) must be taken numerically.

Doing so, and plotting against the classical result in Fig. 1(b), a number of interesting features arise in the self-energy, most of which can be understood by considering the interplay of the dielectric functions of the contacting media;

(i) At very close distances to the metal, in contrast to the classical result, the charge may be repelled from the interface. The reasoning behind this is clear; as $k\to\infty$, as long as $\varepsilon_* > \varepsilon_{\mathrm{M}}$, the charge prefers to reside in the water.
(ii) At intermediate distances, two minima are present, one deeper and closer to the interface and the other much further away. Such a behavior arises from the dielectric function of the metal being much larger than that of water in the intermediate k range, and thus the charge feels an attraction to the interface. In combination with the effect of the repulsive branch described in (i), this results in a minimum in the energy. Such a minimum close to the interface is an interesting finding, as it indicates there may be some universal, purely electrostatic mechanism by which ions can adsorb at a metal electrode.
(iii) At very long distances, the self-energy converges to the classical law, as the dielectric functions tend to their macroscopic values at $k\to 0$.

What is not clear from this analysis is the presence of the small repulsive "bump" further away from the surface. Given that

the model involves just two characteristic lengths, an additional maximum in the profile is unexpected. This has, in the past, been attributed to the presence of an additional repulsive "bound surface charge" contribution to the self-energy, associated with the orientation of dipoles at the interface[23] (in particular, setting the polarization density at the interface, $\tilde{P}_0 = 0\ \mu\mathrm{C\,cm^{-2}}$). Thus, this maximum would physically represent a desolvation-like effect of the interface. However, such an interpretation and physical origin are not clear from the SRA at the interface.

The qualitative presence of an electrostatic minimum close to the interface is interesting and can have some profound consequences within electrochemistry. Quantitatively, however, it does seem rather shallow. The exact depth of the minimum depends strongly on the model parameters, but for it to have any appreciable physical effect, which may correspond to physisorption, the minimum must be on the order of a few k_BT, which it is close to reaching here.

A particular complication, however, is present; examining the form of Eq. (14), a clear problem arises when more complicated pictures of the dielectric response of water are considered. In the denominator of the second term in Eq. (14), once $\varepsilon_{\mathrm{I}}(k)$ is permitted to be negative,[50,51] as is the case when overscreening is considered, the denominator at certain values of K tends to zero, and hence the self-energy diverges. Of course, such a result is unphysical, indicating some fundamental problem behind the SRA. Altogether, this provides the motivation for the work in this paper; by developing a field theoretical model for the two contacting media and then solving the resulting constitutive equations alongside appropriate boundary conditions, a result will be obtained without the shortcomings mentioned above, free of approximations on expressing the dielectric function at the interface, $\varepsilon(z, z';\ R)$.

III. FIELD THEORETICAL APPROACH TO THE METAL–SOLUTION INTERFACE

Now armed with the intuition of what to expect at the metal–solution interface within the SRA, while also being aware of some of its short-comings, a novel method is now presented below to tackle this problem. By defining two bulk free energy functionals that simulate the dielectric response behavior of the two contacting media, constitutive equations can be derived, which can then be solved with appropriate boundary conditions to uncover the electrostatics of the system at hand. In particular, the "novel" description here is in the spirit of a "*novel formulation of nonlocal electrostatics*,"[53] which bypasses the need to solve the complicated integro-differential equations as required within the classical formulation.

The first problem at hand is whether similar results to Sec. II B 2 above can be reproduced by this method, solving the image charge problem for a point charge within this field's theoretical model. Then, to add a touch of realism to the problem, both an external voltage (the electrostatic potential drop between the electrode and the bulk of electrolyte solution), φ_0, and a dipole layer representing chemisorbed water, with polarization density, $\tilde{P}_0$, are introduced to better represent the electrochemical interface in Sec. IV.

A. Free energy functionals in the aqueous solution and the metal

1. Basic equations in an aqueous solution

Let us begin by treating medium I in our problem, the aqueous solution, by constructing a free energy functional inspired by several recent works.[14,54–58] In the grand canonical ensemble, the Landau free energy functional, or grand potential, Φ_G, is defined as

$$\Phi_G = \mathcal{U} - T\mathcal{S} - \sum_i \mu_i N_i, \tag{19}$$

where $\mathcal{U}$ is the internal energy, T is the temperature, $\mathcal{S}$ is the entropy, and μ_i and N_i are the chemical potentials and number of the system components, i.

Within the mean-field approximation, the internal energy of the system can be written as a functional of the electrostatic potential, φ, the free charge density, ϱ_f, and the polarization density field of water, $\mathbf{P}$. To account for polarization fluctuation correlations, $\mathcal{U}$ can be decomposed into "electrostatic" and "correlation" terms such that

$$\mathcal{U}[\varphi, \mathbf{P}, \varrho_{\mathrm{f}}] = \mathcal{U}_{\mathrm{el}}[\varphi, \mathbf{P}, \varrho_{\mathrm{f}}] + \mathcal{U}_{\mathrm{corr}}[\mathbf{P}]. \tag{20}$$

The electrostatic term is constructed by enforcing the modified Poisson equation from the electrostatic energy density, $u_e = \varepsilon_*(\nabla\varphi)^2/8\pi$ (see Refs. 14 and 55), leading to

$$\mathcal{U}_{\mathrm{el}}[\varphi, \mathbf{P}, \varrho_f] = \int_V d\mathbf{r}\left\{-\frac{\varepsilon_*}{8\pi}(\nabla\varphi)^2 + \mathbf{P}\cdot\nabla\varphi + \varrho_{\mathrm{f}}\varphi\right\}, \tag{21}$$

where it is assumed that the system is immersed in some background permittivity of ε_*, thereby introducing the short-range dielectric response as discussed above in the introduction into the system. For an aqueous electrolyte, the free charge density can be written as a first approximation as $\varrho_f(\mathbf{r}) = \varrho_{\mathrm{ext,\,I}} + e\sum_i z_i n_i(\mathbf{r})$, where e is the elementary charge, and z_i and n_i are the valence and ion density of component i. Here, $\varrho_{\mathrm{ext,\,I}}$ is an external charge density sitting in medium I.

Polarization correlations of the solvent water can be conveniently described by some kernel, $\mathcal{K}_{\alpha\beta}(\mathbf{r}, \mathbf{r}')$.[59–61] Most importantly, this kernel can be built to mimic the nonlocal dielectric response function of bulk water. In doing so, this method conveniently avoids any assumptions (e.g., the dielectric approximation[28,62] or the SRA[22,28]) on the dielectric function at the interface while solving the problem directly. This correlation term reads

$$\mathcal{U}_{\mathrm{corr}}[\mathbf{P}] = \frac{2\pi}{\varepsilon_*}\int d\mathbf{r}\int d\mathbf{r}'\ \mathbf{P}_\alpha(\mathbf{r})\mathcal{K}_{\alpha\beta}(\mathbf{r}, \mathbf{r}')\mathbf{P}_\beta(\mathbf{r}'). \tag{22}$$

Here, a Landau–Ginzburg gradient expansion in the polarization density is used to further specify Eq. (22). Using a functional of this kind has a long history in describing confined media.[63–66] For simplicity here, we take the following quadratic form:

$$\mathcal{U}_{\mathrm{corr}}[\mathbf{P}] = \frac{2\pi}{\varepsilon_*}\int d\mathbf{r}\left\{K_1\mathbf{P}^2 + K_2(\nabla\cdot\mathbf{P})^2\right\}, \tag{23}$$

where K_1 and K_2 are the phenomenological coefficients. This first order gradient expansion has been used in the past to mimic the

"Lorentzian" dielectric response[67] and has been sometimes termed the "Marčelja–Radić" functional. Note that it is well known that such a first-gradient expansion is insufficient in reproducing the simulated dielectric response of bulk water;[50,51,68] to do this would require higher order gradient terms in the expansion.[14,54,56–58,60,69]

Entropic contributions to the system can be introduced via a lattice gas approach, which takes the standard form,

$$-T\mathcal{S}[n_i] = k_BT\sum_i \int d\mathbf{r}\; n_i\{\ln(n_i\hat{\Lambda}_i^3) - 1\}, \tag{24}$$

where $\hat{\Lambda}_i$ is the thermal de Broglie wavelength of species i. Finally, writing the last term in Eq. (19) as a function of ion densities such that

$$\left(\sum_i \mu_i N_i\right) = \sum_i \int d\mathbf{r}\; \mu_i n_i \tag{25}$$

completes the construction of the functional. Variational minimization of this functional with respect to the ion density n_i yields

$$z_i e\varphi + k_BT\ln(n_i\hat{\Lambda}_i^3) - \mu_i = 0. \tag{26}$$

Writing in the bulk that $\mu_i = k_BT\ln(n_{b,i}\hat{\Lambda}_i^3)$, where $n_{b,i}$ is the bulk ion density, yields the Boltzmann distribution for the ions,

$$n_i = n_{b,i}\exp\left(-\frac{z_i e\varphi}{k_BT}\right). \tag{27}$$

Assuming a monovalent 1:1 electrolyte, variational minimization of the functional with respect to the electrostatic potential, φ, and the polarization density, $\mathbf{P}$, yields the coupled Euler–Lagrange equations for the electrolyte,

$$\frac{\varepsilon_*}{4\pi}\Delta\varphi - \nabla\cdot\mathbf{P} + \varrho_{\text{ext,I}} - 2en_b\sinh\left(\frac{e\varphi}{k_BT}\right) = 0, \tag{28}$$

$$\varepsilon_*\nabla\varphi + 4\pi(K_1\mathbf{P} - K_2\nabla(\nabla\cdot\mathbf{P})) = 0. \tag{29}$$

To further simplify these, for small electrostatic potentials, $e\varphi/k_BT \ll 1$, and Eq. (28) can be linearized in φ, giving the new set of equations,

$$\frac{1}{4\pi}\Delta\varphi - \frac{1}{\varepsilon_*}\nabla\cdot\mathbf{P} = -\frac{\varrho_{\text{ext,I}}}{\varepsilon_*} + \frac{\kappa_0^2}{4\pi\varepsilon_*}\varphi, \tag{30}$$

$$\nabla\varphi + \frac{4\pi}{\varepsilon_*}(K_1\mathbf{P} - K_2\nabla(\nabla\cdot\mathbf{P})) = 0, \tag{31}$$

where κ_0^{-1} is the vacuum Debye length.

To understand the coupled solvent/electrolyte screening behavior described by such a set of equations, it is appropriate to derive the bulk dielectric function of the system described by such a free energy functional, thus enabling the definition of the set of phenomenological coefficients, $\{K_i\}$, that characterize the dielectric response of water. Indeed, this coupled screening behavior is a tricky problem that is receiving a lot of attention as of late.[70–72] The difficulty in modeling such an interplay arises from competing solvent–solvent and ion–ion correlation effects; at low (millimolar) ion concentrations, solvent correlations will dominate, whereas, in highly concentrated solutions (e.g., solvent-in-salt systems), ion–ion correlations, beyond the Debye mean-field approximation, will take control. Microscopic models of the nonlocal dielectric response of ionic systems have been proposed, leading to a concentration dependent solvent response, as well as the introduction of a wavenumber-dependent inverse Debye length $\kappa_0(k)$.[71–74] Such a procedure, however, is not straightforward and does not result in any simple closed-form expression.

Taking the full Fourier transforms of Eqs. (30) and (31), the dielectric function can be derived as

$$\varepsilon(k) = \left(\varepsilon_* + \frac{\varepsilon_*}{K_1 + K_2k^2}\right) + \frac{\kappa_0^2}{k^2}, \tag{32}$$

which, for $K_1 = 1/(\gamma-1)$ and $K_2 = \gamma\Lambda^2/(\gamma-1)$, leads to the term in the brackets resembling Eq. (15). Such a simple expression coupling the nonlocal solvent response to the electrolyte ion correlations arises from the mean-field approximation used in this work and has previously been proposed as an interpolation formula decades ago.[75] Note that at small k, when $\varepsilon(k)\to\varepsilon$, the second term in Eq. (32) diverges as $\sim k^{-2}$, thus altogether yielding the classical Debye screening behavior. On the contrary, at large k, the second term vanishes, and the dielectric response is determined by the solvent. This formula becomes exact in the limit of small k and small electrolyte concentrations, where κ_0^{-1} is much smaller than any characteristic solvent correlation length. Thus, this constructed functional should perform reasonably well for diluted electrolyte solutions, given the assumptions of both linear dielectric response and the Debye–Hückel approximation used here.

Constitutive equations: Returning to Eqs. (30) and (31), it is clear that the right-hand side of Eq. (30) is associated with only the free charge of the system, ϱ_f. Thus, it can be written as $\nabla\cdot\mathbf{D}$, where $\mathbf{D}$ is the displacement field. Using this and integrating Eq. (30) once yields the constitutive relationship of electrostatics,

$$\mathbf{D} = -\varepsilon_*\nabla\varphi + 4\pi\mathbf{P}. \tag{33}$$

As with the electric field, a new potential, ψ, can be introduced, defined to be associated purely with the displacement field. Given that in the static limit, the transverse components of the fields are zero, this potential can be defined simply as

$$\mathbf{D} = -\nabla\psi. \tag{34}$$

Plugging this into Eq. (33) yields

$$4\pi\mathbf{P} = \nabla(\varepsilon_*\varphi - \psi). \tag{35}$$

Thus, the set of Euler–Lagrange equations defined in Eqs. (30) and (31) can be reformulated in terms of the two potentials φ and ψ,

$$\Delta\psi + 4\pi\varrho_{\text{ext,I}} - \varepsilon\kappa^2\varphi = 0, \tag{36}$$

$$\psi = \varepsilon\left\{\left(1+\gamma\kappa^2\Lambda^2\right)\varphi - \Lambda^2\left(\frac{4\pi}{\varepsilon_*}\varrho_{\text{ext,I}} + \Delta\varphi\right)\right\}, \tag{37}$$

where $\kappa = \kappa_0/\sqrt{\varepsilon}$ is the inverse Debye length in water. These equations then define the new *constitutive relations* for the electrolyte

solution. Note that solving for both φ and ψ will yield the three fields, **D**, **E**, and **P**, thus allowing the exact determination of boundary conditions when an interface is considered.

2. Basic equations in a Thomas–Fermi metal

In a similar way to the electrolyte, the electrostatic energy in the metal can be written as

$$\mathcal{U}_{\rm el}[\varphi,\varrho_f] = \int d\mathbf{r}\left\{-\frac{\varepsilon_{\rm M}}{8\pi}(\nabla\varphi)^2 + (\varrho_{\rm TF}+\varrho_{\rm ext,\,II})\varphi\right\}, \tag{38}$$

where $\varrho_{\rm TF}$ is the induced charge density of electrons to an external charge distribution, $\varrho_{\rm ext,\,II}$. Variational minimization with respect to the electrostatic potential yields the Poisson equation in the metal,

$$\varepsilon_{\rm M}\Delta\varphi + 4\pi\varrho_{\rm TF} + 4\pi\varrho_{\rm ext,II} = 0. \tag{39}$$

The linear approximation for TF screening theory yields for the induced charge distribution,

$$4\pi\varrho_{\rm TF} = -\varepsilon_{\rm M}\varkappa_{\rm TF}^2\varphi. \tag{40}$$

Similarly associating the displacement field **D**, and hence its potential, ψ, with the free external and the induced charge densities yields the constitutive equations in the metal,

$$\Delta\psi = -4\pi\varrho_{\rm ext,\,II} + \varepsilon_{\rm M}\varkappa_{\rm TF}^2\varphi, \tag{41}$$

$$\varepsilon_{\rm M}\Delta\varphi = -4\pi\varrho_{\rm ext,\,II} + \varepsilon_{\rm M}\varkappa_{\rm TF}^2\varphi, \tag{42}$$

revealing a surprisingly simple relationship between ψ and φ in the metal. Note that these expressions reproduce the screening behavior described by Eq. (16).

B. Introducing a point charge: Solving the image charge problem

Having derived the constitutive equations in both media, let us now try to solve them for the case of a charge at an interface. To begin, we will approach the problem with a simplistic model of the system, neglecting any effects of external potential or adsorbed water at the interface. While this may remove a sense of realism from the model, such a model will provide some preliminary results to compare to previous works before the introduction of these complicating factors, which will be considered in Sec. IV.

Regardless of the model, the constitutive equations must first be setup to account for the geometry of the problem, and the charge distributions, $\varrho_{\rm ext,I}$ and $\varrho_{\rm ext,II}$, must be defined according to the method of images. These unknown charge distributions can then be solved by imposing the Maxwell boundary conditions at the interface. As will be shown, introducing this new potential, ψ, associated with the displacement field **D**, will dramatically simplify the problem.

Consider the setup of the system in Fig. 1(a); an ion is placed at a distance of $z = a$ away from the interface at $z = 0$. The system is translationally invariant in the xy-plane; thus, a cylindrical coordinate system can be used here, with the z-axis normal to the plane of the interface. It is then convenient to consider the *Fourier–Bessel* transform of the potentials, $\tilde{\psi} \equiv \tilde{\psi}(z,K)$ and $\tilde{\varphi} \equiv \tilde{\varphi}(z,K)$, where K is the radial wavevector, related to the real space potentials by

$$\varphi(z,R) = \frac{1}{2\pi}\int_0^\infty KdK\,J_0(KR)\tilde{\varphi}(z,K), \tag{43}$$

$$\psi(z,R) = \frac{1}{2\pi}\int_0^\infty KdK\,J_0(KR)\tilde{\psi}(z,K). \tag{44}$$

Writing the Laplacian operator as its Fourier–Bessel analog, $\Delta = \partial_z^2 - K^2$, the constitutive equations in the solution are then given by

$$\left[\partial_z^2 - K^2\right]\tilde{\psi}_{\rm I}^{z\geq 0} = -4\pi\tilde{\varrho}_{\rm ext,I} + \varepsilon\kappa^2\tilde{\varphi}_{\rm I}^{z\geq 0}, \tag{45}$$

$$\tilde{\psi}_{\rm I}^{z\geq 0} = \varepsilon\left\{\left(1+\gamma\kappa^2\Lambda^2\right)\tilde{\varphi}_{\rm I}^{z\geq 0} - \Lambda^2\left(\frac{4\pi}{\varepsilon_*}\tilde{\varrho}_{\rm ext,I} + \left[\partial_z^2 - K^2\right]\tilde{\varphi}_{\rm I}^{z\geq 0}\right)\right\}, \tag{46}$$

and in the metal by

$$\left[\partial_z^2 - K^2\right]\tilde{\psi}_{\rm II}^{z<0} = -4\pi\tilde{\varrho}_{\rm ext,II} + \varepsilon_{\rm M}\varkappa_{\rm TF}^2\tilde{\varphi}_{\rm II}^{z<0}, \tag{47}$$

$$\varepsilon_{\rm M}\left[\partial_z^2 - K^2\right]\tilde{\varphi}_{\rm II}^{z<0} = -4\pi\tilde{\varrho}_{\rm ext,II}^{z<0} + \varepsilon_{\rm M}\varkappa_{\rm TF}^2\tilde{\varphi}_{\rm II}^{z<0}, \tag{48}$$

where $\tilde{\varrho}_{{\rm ext},i} \equiv \tilde{\varrho}_{{\rm ext},i}(z,K)$. Let us consider these external charge distributions more carefully. As in the method of images, if a charge is introduced at an interface, to correctly solve for the electrostatic potential, two additional fictitious charges must be placed such that $\varrho_{\rm ext,I} = \varrho^{(0)} + \varrho'$ and $\varrho_{\rm ext,II} = \varrho''$, where $\varrho^{(0)}$ is the contribution from the real point charge, and ϱ', ϱ'' are the images. However, as both of the media are now nonlocal, it is not necessarily correct to consider them as point charges. Rather, they will have some distribution in space. Hence, assuming that this distribution sits only in the lateral plane, the Fourier–Bessel transforms of the external charge densities in both media can be written as

$$\tilde{\varrho}_{\rm ext,\,I}(z,K) = q\delta(z-a) + q\mathcal{U}(K)\delta(z+a), \tag{49}$$

$$\tilde{\varrho}_{\rm ext,II}(z,K) = q\mathcal{V}(K)\delta(z-a), \tag{50}$$

where $\mathcal{U}$ and $\mathcal{V}$ are the "unknown" charge distributions that must be solved for. To find these, following the method of images, the potentials φ and ψ must first be found by solving the constitutive equations. Inserting the external charge distributions as defined in Eqs. (49) and (50) into Eqs. (45)–(48), the electrostatic potentials can then be written in the aqueous solution as

$$\begin{aligned}\tilde{\varphi}_{\rm I}^{z\geq 0}(z,K) = {}& \frac{2\pi q}{\varepsilon}\left(\frac{g_1}{\tilde{Q}_1}e^{-\tilde{Q}_1|z-a|} + \frac{g_2}{\tilde{Q}_2}e^{-\tilde{Q}_2|z-a|}\right)\\ &+ \frac{2\pi q}{\varepsilon}\mathcal{U}(K)\left(\frac{g_1}{\tilde{Q}_1}e^{-\tilde{Q}_1(z+a)} + \frac{g_2}{\tilde{Q}_2}e^{-\tilde{Q}_2(z+a)}\right),\end{aligned} \tag{51}$$

$$\begin{aligned}\tilde{\psi}_{\rm I}^{z\geq 0}(z,K) = {}& 2\pi q\left(\frac{h_1}{\tilde{Q}_1}e^{-\tilde{Q}_1|z-a|} + \frac{h_2}{\tilde{Q}_2}e^{-\tilde{Q}_2|z-a|}\right)\\ &+ 2\pi q\mathcal{U}(K)\left(\frac{h_1}{\tilde{Q}_1}e^{-\tilde{Q}_1(z+a)} + \frac{h_2}{\tilde{Q}_2}e^{-\tilde{Q}_2(z+a)}\right),\end{aligned} \tag{52}$$

and in the metal as

$$\tilde{\varphi}_{\mathrm{II}}^{z<0}(z,K) = \frac{2\pi q}{\varepsilon_{\mathrm{M}}}\mathcal{V}(K)\frac{e^{\sqrt{K^2+\varkappa_{\mathrm{TF}}^2}(z-a)}}{\sqrt{K^2+\varkappa_{\mathrm{TF}}^2}}, \tag{53}$$

$$\tilde{\psi}_{\mathrm{II}}^{z<0}(z,K) = 2\pi q\,\mathcal{V}(K)\frac{e^{\sqrt{K^2+\varkappa_{\mathrm{TF}}^2}(z-a)}}{\sqrt{K^2+\varkappa_{\mathrm{TF}}^2}}, \tag{54}$$

where the coefficients in $\tilde{\varphi}_I$ are given by

$$g_1 = \frac{\gamma\Lambda^2Q_1^2-1}{\sqrt{\left(1-2\kappa\Lambda+\gamma\kappa^2\Lambda^2\right)\left(1+2\kappa\Lambda+\gamma\kappa^2\Lambda^2\right)}}, \tag{55}$$

$$g_2 = \frac{1-\gamma\Lambda^2Q_2^2}{\sqrt{\left(1-2\kappa\Lambda+\gamma\kappa^2\Lambda^2\right)\left(1+2\kappa\Lambda+\gamma\kappa^2\Lambda^2\right)}}, \tag{56}$$

leading to the definitions of the coefficients in $\tilde{\psi}_{\mathrm{I}}$,

$$h_1 = g_1\Lambda^2Q_2^2, \qquad h_2 = g_2\Lambda^2Q_1^2. \tag{57}$$

Here, the characteristic parameters of the solutions, $Q_{1,2}$ (which have dimensionality of inverse length), are defined as

$$Q_1 = \frac{1}{\sqrt{2}}\sqrt{\gamma\kappa^2+\frac{1}{\Lambda^2}\left(1+\sqrt{\left(1-2\kappa\Lambda+\gamma\kappa^2\Lambda^2\right)\left(1+2\kappa\Lambda+\gamma\kappa^2\Lambda^2\right)}\right)}, \tag{58}$$

$$Q_2 = \frac{1}{\sqrt{2}}\sqrt{\gamma\kappa^2+\frac{1}{\Lambda^2}\left(1-\sqrt{\left(1-2\kappa\Lambda+\gamma\kappa^2\Lambda^2\right)\left(1+2\kappa\Lambda+\gamma\kappa^2\Lambda^2\right)}\right)}, \tag{59}$$

and the radial wavevector, K, couples with $Q_{1,2}$ as $\tilde{Q}_{1,2} = \sqrt{K^2+Q_{1,2}^2}$. Note that in the classical limit, i.e., $\gamma \to 1$ and $\Lambda \to \infty$, these definitions reduce to $Q_1 \to \kappa$ and $Q_2 \to 0$. Following the method of images, the Maxwell boundary conditions can be applied here to solve for $\mathcal{U}(K)$ and $\mathcal{V}(K)$. First, let us consider the displacement field; before, within the nonlocal electrostatics formulation, such a condition on $\mathbf{D}$ resulted in non-trivial integro-differential equations to solve. Here, however, the boundary condition can be written explicitly through the potential ψ, thus giving

$$(\mathbf{D_I}-\mathbf{D_{II}})\cdot\hat{\mathbf{n}} = -\partial_z\tilde{\psi}_{\mathrm{I}}(z=0,K)+\partial_z\tilde{\psi}_{\mathrm{II}}(z=0,K) = 0. \tag{60}$$

Note that here there is no external charge localized on the interface, and so the displacement field is continuous. The second boundary condition is on the electrostatic potential; in the absence of dipoles at the interface, the potential is also continuous,

$$\tilde{\varphi}_{\mathrm{I}}(z=0,K)-\tilde{\varphi}_{\mathrm{II}}(z=0,K) = 0. \tag{61}$$

Together, these boundary conditions yield the following solutions for $\mathcal{U}$ and $\mathcal{V}$:

$$\mathcal{U}(K) = \frac{\xi\left(h_1e^{-\tilde{Q}_1a}+h_2e^{-\tilde{Q}_2a}\right)-\sqrt{K^2+\varkappa_{\mathrm{TF}}^2}\left(\frac{g_1}{\tilde{Q}_1}e^{-\tilde{Q}_1a}+\frac{g_2}{\tilde{Q}_2}e^{-\tilde{Q}_2a}\right)}{\xi\left(h_1e^{-\tilde{Q}_1a}+h_2e^{-\tilde{Q}_2a}\right)+\sqrt{K^2+\varkappa_{\mathrm{TF}}^2}\left(\frac{g_1}{\tilde{Q}_1}e^{-\tilde{Q}_1a}+\frac{g_2}{\tilde{Q}_2}e^{-\tilde{Q}_2a}\right)}, \tag{62}$$

$$\mathcal{V}(K) = \frac{2\sqrt{K^2+\varkappa_{\mathrm{TF}}^2}\left(h_1e^{-\tilde{Q}_1a}+h_2e^{-\tilde{Q}_2a}\right)\left(\frac{g_1}{\tilde{Q}_1}e^{-\tilde{Q}_1a}+\frac{g_2}{\tilde{Q}_2}e^{-\tilde{Q}_2a}\right)}{\xi\left(h_1e^{-\tilde{Q}_1a}+h_2e^{-\tilde{Q}_2a}\right)+\sqrt{K^2+\varkappa_{\mathrm{TF}}^2}\left(\frac{g_1}{\tilde{Q}_1}e^{-\tilde{Q}_1a}+\frac{g_2}{\tilde{Q}_2}e^{-\tilde{Q}_2a}\right)} \times e^{a\sqrt{K^2+\varkappa_{\mathrm{TF}}^2}}, \tag{63}$$

where $\xi = \varepsilon/\varepsilon_{\mathrm{M}}$. Acknowledging that the first term in Eq. (51) is the potential created by the point charge, $\tilde{\varphi}^{(0)}$, the self-energy is then given by plugging Eq. (51) into Eq. (5), yielding

$$W(a) = \frac{q^2}{2\varepsilon}\int_0^\infty KdK\,\mathcal{U}(K)\left(\frac{g_1}{\tilde{Q}_1}e^{-2\tilde{Q}_1a}+\frac{g_2}{\tilde{Q}_2}e^{-2\tilde{Q}_2a}\right). \tag{64}$$

Given the complexity of $\mathcal{U}$, the integral over K can only be taken numerically. Regardless, this expression is a first attempt at answering the question underpinning this paper, tackling the image charge problem for a charge at the metal–solution interface.

1. Pure water limit

To begin, let us first consider the pure water limit, without complicating the problem with ionic screening. In this case, Eq. (64) simplifies significantly. As $\kappa \to 0$ Å^{-1} in the pure water limit, $\tilde{Q}_1 \to \sqrt{K^2+1/\Lambda^2}$, $\tilde{Q}_2 \to K$, $g_1 \to \gamma-1$, $g_2 \to 1$, $h_1 \to 0$, and $h_2 \to 1$. Thus, the expression for the self-energy in the pure water limit reduces to

$$W(a) = \frac{q^2}{2\varepsilon}\int_0^\infty dK\,\mathcal{U}_{\mathrm{pure}}(K)\left(e^{-2Ka}+\frac{K(\gamma-1)}{\sqrt{K^2+1/\Lambda^2}}e^{-2a\sqrt{K^2+1/\Lambda^2}}\right), \tag{65}$$

where

$$\mathcal{U}_{\mathrm{pure}}(K) = \frac{\xi Ke^{-Ka}-\sqrt{K^2+\varkappa_{\mathrm{TF}}^2}\left(e^{-Ka}+\frac{K(\gamma-1)}{\sqrt{K^2+1/\Lambda^2}}e^{-a\sqrt{K^2+1/\Lambda^2}}\right)}{\xi Ke^{-Ka}+\sqrt{K^2+\varkappa_{\mathrm{TF}}^2}\left(e^{-Ka}+\frac{K(\gamma-1)}{\sqrt{K^2+1/\Lambda^2}}e^{-a\sqrt{K^2+1/\Lambda^2}}\right)}. \tag{66}$$

With these expressions, it is useful to first consider the limiting cases to ensure that the model is working as expected.

Classical self-energy law: As a first check, let us reproduce the limiting law for the classical dielectric/dielectric interface. From Eqs. (65) and (66), this limit is obtained by setting $\gamma \to 1$ in medium I and $\varkappa_{\mathrm{TF}} \to 0$ in medium II, thus representing an interface between dielectrics with dielectric constants of ε and ε_{M}. In this case,

$$W(a) = \frac{q^2}{4\varepsilon a}\left(\frac{\xi-1}{\xi+1}\right), \tag{67}$$

and the classical limiting law as in Eq. (6) is obtained. If medium II is a conductor, $\xi \to 0$, and this law simplifies to Eq. (7).

Conductor/nonlocal dielectric interface: Before considering the full complexity of TF screening in the metal, let us again treat it as a conductor to see how nonlocality in the water may affect the law of self-energy. Taking the limit of $\xi \to 0$, Eqs. (65) and (66) yield for the self-energy,

$$W(a) = -\frac{q^2}{4\varepsilon a}\left\{1+(\gamma-1)e^{-2a/\Lambda}\right\}. \tag{68}$$

Close to the interface, in the limit where $2a \ll \Lambda$ and $W(a) \approx -q^2/4\varepsilon_* a$. This behavior is expected; in the short range, the dielectric response of the Lorentzian dielectric function becomes that of the short-range dielectric constant, ε_*. Far from the interface, $2a \gg \Lambda$, this law tends to be the classical one. Thus, this law describes a smooth interpolation between the classical self-energy laws with macroscopic and short-range dielectric constants.

TF metal/dielectric interface: Another limiting case that can be analyzed from this expression is the interface between the TF metal and classical, macroscopic water. This has been studied many times in the past,[21,22,27] as well as in more recent works,[76,77] and so it will be a gratifying validation of the model here if the result is reproduced. Taking the limit $\gamma \to 1$,

$$W(a) = \frac{q^2}{2\varepsilon}\int_0^\infty dK e^{-2Ka}\left(\frac{\xi K - \sqrt{K^2+\varkappa_{\mathrm{TF}}^2}}{\xi K + \sqrt{K^2+\varkappa_{\mathrm{TF}}^2}}\right), \tag{69}$$

which is equivalent to the expression derived explicitly in Ref. 21.

TF metal/Lorentzian water interface: Now, with a better understanding of the expression and its limiting behavior, the self-energy profile of an ion at the TF metal–Lorentzian water interface is plotted in Fig. 2, alongside all the limiting cases considered above.

Qualitatively, the profile calculated here is similar to that calculated in Sec. II B 2 within the SRA. Close to the interface, there is a minimum in the self-energy, resulting from the repulsive contribution becoming significant as the field of the charge penetrates the metal. This again indicates a purely electrostatic mechanism by which ions adsorb at the electrochemical interface, although here the result is obtained via a more rigorous consideration of the boundary conditions.

This minimum is, however, very sensitive to the model parameters. For $\varepsilon_* = 5$, the minimum is only ~1 k_BT deep; while not seemingly significant, it is enough to induce an absorption effect. However, reducing ε_* to 3, the minimum deepens significantly to ~14 k_BT. This effect makes intuitive sense; consider the arguments laid out above for the classical case. At the interface, the dielectric constant is close to ε_*. If $\varepsilon_*/\varepsilon_{\mathrm{M}} < 1$, the charge will always be attracted to the interface as shown in Fig. 2. Conversely, as this ratio becomes increasingly larger than 1, the repulsive contribution to the self-energy strengthens closer to the interface, and so the minimum becomes shallower.

The TF screening length has a similar qualitative effect, which can be seen in Fig. 2(c). For large screening lengths (small $\varkappa_{\mathrm{TF}}$), the metal is seen by our test charge as a dielectric with dielectric constant ε_{M} at short distances from the interface, and thus the charge is repelled, as $\varepsilon_* > \varepsilon_{\mathrm{M}}$. As the screening length decreases ($\varkappa_{\mathrm{TF}}$ increases), the metal becomes a better conductor, and so the minimum will deepen and be drawn closer to the interface as the field produced by the charge gets very quickly screened within the metal.

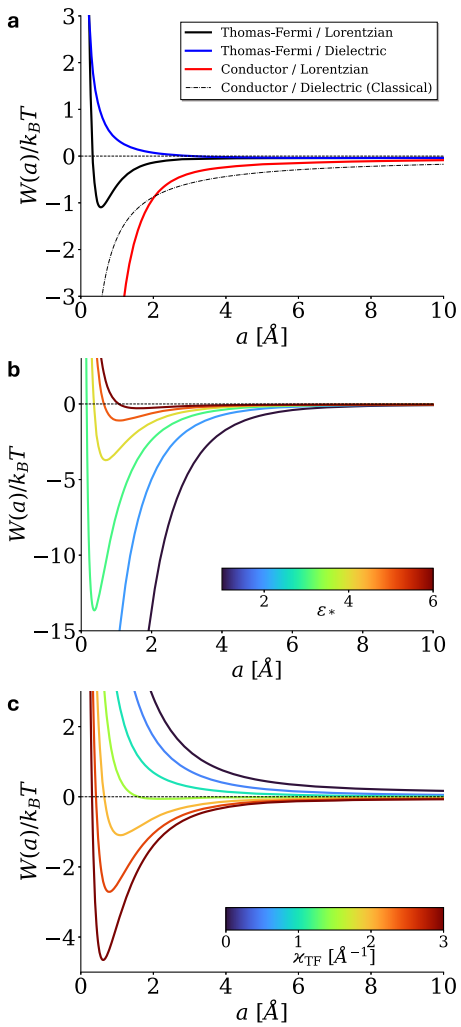

FIG. 2. Self-energy profiles of a point charge at a metal–water interface. (a) Self-energy for a charge at different interfaces plotted from Eq. (5.77). For the TF metal, the parameters used are $\varepsilon_{\mathrm{M}} = 2$ and $\varkappa_{\mathrm{TF}} = 2$ Å^{-1}, and for the nonlocal Lorentzian model, the parameters used are $\varepsilon = 80$, $\varepsilon_* = 5$, and $\Lambda = 3$ Å. For a conductor, $\varepsilon_{\mathrm{M}} \to \infty$, and for the dielectric, $\gamma = \varepsilon/\varepsilon_* \to 1$. (b) Dependence of the self-energy on the short-range dielectric constant for the TF metal–Lorentzian water interface. Values of ε_* range from 1 to 6, indicated by the color bar. (c) Dependence of the self-energy on the TF screening length for the TF metal/Lorentzian water interface. The results are displayed for the values of $\varkappa_{\mathrm{TF}}$ from 0 to 3 Å^{-1}, indicated by the color bar.

2. Effect of aqueous electrolyte

Having established that this adsorption minimum arises purely as an effect of the coupling between the nonlocal effects of the Lorentzian water and the TF metal, the effect of background electrolyte screening can now be investigated via Eqs. (62) and (64). As above, it is informative to investigate the limiting laws of the self-energy. In the local, classical limit, $\gamma \to 1$, $\xi \to 0$, and Eq. (64) becomes

$$W(a) = -\frac{q^2}{4\varepsilon a}e^{-2\kappa a}. \tag{70}$$

This simple equation describes a consistently attractive image contribution to the self-energy, which becomes weaker with higher background electrolyte concentration due to the additional exponential screening factor. Of course, within this linear Debye–Hückel approximation, strictly only small concentrations up to ~100 mM

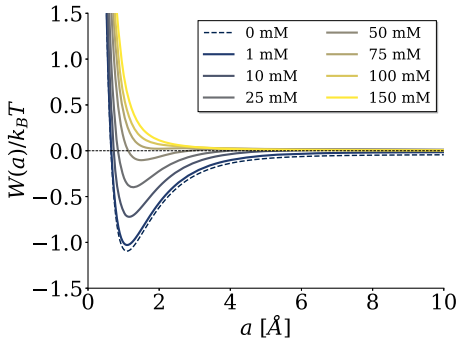

FIG. 3. Dependence of the adsorption minimum on the background electrolyte concentration at the pzc. Self-energy profiles plotted from Eq. (64) for the indicated concentrations, at the pzc, $\varphi_0 = 0$ mV. The TF parameters here are $\varepsilon_M = 2$ and $\varkappa_{TF} = 2$ Å^{-1}, and the Lorentzian parameters are $\varepsilon = 80$, $\varepsilon_* = 5$, and $\Lambda = 3$ Å.

can be considered.[75] However, how will such a behavior affect the adsorption minimum that arises when nonlocality of the water is considered?

For small concentrations on the order of ~1 mM, the self-energy profile, plotted in Fig. 3, is largely unaffected. However, in increasing the electrolyte concentration, the attractive branch is screened more strongly, and the minimum diminishes, disappearing altogether at ~75 mM. Above these concentrations, the point charge is completely repelled from the interface, thereby revealing a *negative adsorption* effect (i.e., ions extruding into the bulk), providing a mechanism by which this phenomenon may occur.

Reproducing the primary qualitative results above of the SRA in Ref. 22 for the TF metal/Lorentzian water interface serves as a reasonable validation of this approach. Moreover, the presented formalism acts as a starting point, upon which further complexity can be added to the model. For example, one qualitative feature not reproduced here is the repulsive barrier present within the SRA. This prompts the following question: What does this approximation implicitly introduce that is not considered above, and are they physical?

Of course, what we have considered thus far in the field theory is a very crude representation of the electrochemical interface. There will be additional electrostatic effects stemming from chemisorbed water at the interface, which generates surface polarization, $\tilde{P}_0$ (see Refs. 14 and 54). Similarly, the electrochemical interface can be influenced by an external voltage, φ_0, which was not considered above or in the literature. Such effects can be introduced in a reasonably straightforward way through this theoretical framework, as will be shown below.

IV. SURFACE EFFECTS: ELECTRODE POTENTIAL AND CHEMISORBED WATER

In all results presented above, it was assumed that only the point charge sitting at $z = a$ contributes to the electrostatic potential distribution. Of course, such an assumption massively simplifies the system; for example, an external voltage applied to the electrode, or even the presence of water chemisorbed to the metal surface, will also contribute to the potential distribution, thereby influencing what the ion in question may feel. In this section, we introduce these effects to investigate the interface within this model, thus accounting for these effects, yielding a more complete and realistic answer to the question underlying this paper.

A. Electrostatic potential distribution at the electrochemical interface

In the absence of the point charge, the external charge distributions in both media can be neglected, i.e., $\varrho_{\text{ext},i} = 0$. Thus, the geometry of the system simply becomes planar, and the operators in the constitutive equations can be simplified to 1D. This then allows the constitutive equations to be written as

$$\partial_z^2 \psi_{\text{I}}^{z\geq 0} - \varepsilon\kappa^2 \varphi_{\text{I}}^{z\geq 0} = 0, \tag{71}$$

$$\psi_{\text{I}}^{z\geq 0} = \varepsilon\left\{\left(1 + \gamma\kappa^2\Lambda^2\right)\varphi_{\text{I}}^{z\geq 0} - \Lambda^2\partial_z^2\varphi_{\text{I}}^{z\geq 0}\right\}. \tag{72}$$

Inserting Eq. (72) into(71) yields a fourth order differential equation to solve for φ_I,

$$\Lambda^2\partial_z^4\varphi_{\text{I}}^{z\geq 0} - (1 + \gamma\kappa^2\Lambda^2)\partial_z^2\varphi_{\text{I}}^{z\geq 0} + \kappa^2\varphi_{\text{I}}^{z\geq 0} = 0, \tag{73}$$

Defining the electrostatic potential here in the bulk of the electrolyte solution to be zero, i.e., $\varphi_{\text{I}}(z \to \infty) = 0$, as well as the electric field, $E_z = -\partial_z\varphi_{\text{I}}(z \to \infty) = 0$, leads to the following general solution of Eq. (73):

$$\varphi_{\text{I}}^{z\geq 0}(z) = c_1 e^{-Q_1 z} + c_2 e^{-Q_2 z}, \tag{74}$$

where $c_{1,2}$ are unknown coefficients and the characteristic lengths $Q_{1,2}$ are defined as in Eqs. (58) and (59). Plugging Eq. (74) into (72) yields the expression for $\psi_{\text{I}}^{z\geq 0}$,

$$\psi_{\text{I}}^{z\geq 0}(z) = \varepsilon\kappa^2\left(\frac{c_1}{Q_1^2}e^{-Q_1 z} + \frac{c_2}{Q_2^2}e^{-Q_2 z}\right). \tag{75}$$

In the metal, again the geometry of the system allows us to simplify the operators to 1D, and in the absence of the external charges, $\varrho_{\text{ext,II}} = 0$. However, here the effect of a constant external potential, φ_0, relative to the bulk of the solution phase, must be accounted for. This can quite easily be done by writing φ as $\varphi_{\text{II}} - \varphi_0$ in Eq. (40), giving

$$\partial_z^2\psi_{\text{II}}^{z<0} - \varepsilon_{\text{M}}\varkappa_{\text{TF}}^2(\varphi_{\text{II}}^{z<0} - \varphi_0) = 0, \tag{76}$$

$$\partial_z^2\varphi_{\text{II}}^{z<0} - \varkappa_{\text{TF}}^2(\varphi_{\text{II}}^{z<0} - \varphi_0) = 0. \tag{77}$$

The general solution that satisfies these equations is

$$\varphi_{\text{II}}^{z<0}(z) = \varphi_0 - (\varphi_0 - \varphi_S)e^{\varkappa_{\text{TF}} z}, \tag{78}$$

$$\psi_{\text{II}}^{z<0}(z) = \varepsilon_{\text{M}}\left[\varphi_0 - (\varphi_0 - \varphi_S)e^{\varkappa_{\text{TF}} z}\right], \tag{79}$$

where again an unknown constant, φ_S, representing the electrostatic potential on the metal side of the interface, i.e., at $z = -0$, has been introduced.

1. Maxwell boundary conditions and solutions

The general solutions laid out in Eqs. (74), (75), and (78) involve three unknown constants; these must be solved for by applying three boundary conditions at the interface. The first of these boundary conditions, as above in Sec. III B, is on the displacement field. By explicitly introducing an external potential, φ_0, the charge on the electrode is delocalized throughout the metal and is, therefore, not localized at the interface. Thus, the boundary condition for the continuity of the displacement field holds as

$$\hat{\mathbf{n}} \cdot (\mathbf{D_I} - \mathbf{D_{II}}) = -\partial_z \psi_{\mathrm{I}}(z=0) + \partial_z \psi_{\mathrm{II}}(z=0) = 0. \tag{80}$$

We now, however, wish to also consider the effect of water chemisorbed at the interface. By treating the water as a dipole sheet of thickness d, it is clear that the electrostatic potential will no longer be continuous. Instead, there will be a "dipole drop" over the interface, written as

$$\varphi_{\mathrm{I}}(z=0) - \varphi_{\mathrm{II}}(z=0) = \frac{4\pi}{\varepsilon_*}\bar{P}_0 d, \tag{81}$$

where $\bar{P}_0$ is the polarization density normal to the interface, which represents the orientation of the water dipoles. A natural question that arises here is the appropriate value to assign to d. The maximum thickness of the dipole layer here is the diameter of a water molecule ($d_{\max} \approx 2.5$ Å), when all of the water dipoles point in the direction of the normal vector to the interface, corresponding to a maximum polarization density of $\bar{P}_{0,\max} \approx 20 - 30\ \mu\mathrm{C\,cm^{-2}}$, corresponding to a surface density of ~10–15 molecules per nm^2. Then, we can simply approximate the thickness of the dipole layer to be $d \approx (\bar{P}_0/\bar{P}_{0,\max})d_{\max}$. Prescribing a given polarization density normal to the interface leads to the third boundary condition; using Eq. (35), the normal component of the polarization density can be defined to be equal to $\bar{P}_0$ at the interface,

$$\hat{\mathbf{n}} \cdot \mathbf{P}(z=0) = \frac{1}{4\pi}\left[\varepsilon_* \partial_z \varphi_{\mathrm{I}}(z=0) - \partial_z \psi_{\mathrm{I}}(z=0)\right] = \bar{P}_0. \tag{82}$$

These three boundary conditions yield the following solutions:

$$c_1(\varphi_0, \bar{P}_0) = -Q_1 \frac{\frac{4\pi}{\varepsilon_*}\bar{P}_0\left(Q_2\varkappa_{\mathrm{TF}}(1+Q_2 d) + \kappa^2(\xi - \varkappa_{\mathrm{TF}}\gamma d)\right) + \left(Q_2^2 - \gamma\kappa^2\right)\varkappa_{\mathrm{TF}}\varphi_0}{(Q_1 - Q_2)\left(\varkappa_{\mathrm{TF}}Q_1Q_2 + \kappa^2(\xi(Q_1+Q_2) + \gamma\varkappa_{\mathrm{TF}})\right)}, \tag{83}$$

$$c_2(\varphi_0, \bar{P}_0) = Q_2 \frac{\frac{4\pi}{\varepsilon_*}\bar{P}_0\left(Q_1\varkappa_{\mathrm{TF}}(1+Q_1 d) + \kappa^2(\xi - \varkappa_{\mathrm{TF}}\gamma d)\right) + \left(Q_1^2 - \gamma\kappa^2\right)\varkappa_{\mathrm{TF}}\varphi_0}{(Q_1 - Q_2)\left(\varkappa_{\mathrm{TF}}Q_1Q_2 + \kappa^2(\xi(Q_1+Q_2) + \gamma\varkappa_{\mathrm{TF}})\right)}, \tag{84}$$

$$\varphi_S(\varphi_0, \bar{P}_0) = \frac{-\frac{4\pi}{\varepsilon_*}\bar{P}_0\xi\kappa^2(1 + (Q_1+Q_2)d) + \left(Q_1Q_2 + \gamma\kappa^2\right)\varkappa_{\mathrm{TF}}\varphi_0}{\varkappa_{\mathrm{TF}}Q_1Q_2 + \kappa^2(\xi(Q_1+Q_2) + \gamma\varkappa_{\mathrm{TF}})}. \tag{85}$$

Then, with these definitions, plotting Eqs. (74) and (78) in Fig. 4 shows how the electrostatic potential is distributed across the interface. First, let us consider the case when all the dipoles are pointing parallel to the interface such that $\bar{P}_0 = 0\ \mu\mathrm{C\,cm^{-2}}$ and $d = 0$ Å. In this case, in Fig. 4(b), the external voltage drives an electrostatic potential distribution across the interface, which is screened more quickly the higher the electrolyte concentration. Note that a "double layer" is formed in both the electrolyte (due to ions) and the metal (due to electrons).

In Fig. 4(c), the external voltage is set to zero, and only the effect of chemisorbed water is considered. In the absence of electrolyte in the pure water limit, $\kappa \to 0$, the dipoles create a potential distribution, which decays with characteristic length Λ. Note that this field does not decay to zero—in the absence of electrolyte screening, Eq. (74) reveals that the potential instead tends to a non-zero value, given by

$$\varphi_{\kappa=0}(z \to \infty) = \frac{4\pi}{\varepsilon_*}\bar{P}_0(\Lambda + d), \tag{86}$$

a direct result of introducing unscreened "bound charge" in medium I. Upon introducing the electrolyte, it is clear that the presence of this bound charge at the interface is sufficient to drive the formation of a double layer in the solution, as indicated first by Belaya and Levadny.[78,79]

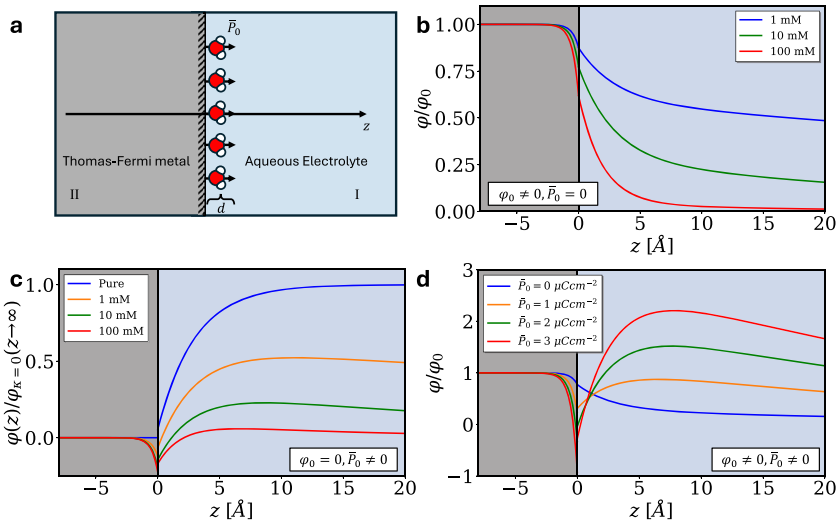

FIG. 4. Electrostatic potential distribution for two media in contact. (a) Sketch of the system, showing the interface at $z = 0$, and a dipole layer due to chemisorbed water of thickness, d, leading to a polarization density of $\bar{P}_0$. Panels (b)–(d) show the potential distribution across the interface, as calculated by Eqs. (74) and (78). In all plots, unless otherwise stated, $\varepsilon = 80$, $\varepsilon_* = 5$, and $\varepsilon_{\mathrm{M}} = 2$ such that $\gamma = 80/5 = 16$ and $\xi = 80/2 = 40$, and the characteristic lengths are $\Lambda = 3$ Å and $\varkappa_{\mathrm{TF}} = 2$ Å^{-1}. In panel (b), $\bar{P}_0 = 0\ \mu\mathrm{C\,cm^{-2}}$; in panel (c), $\varphi_0 = 0$ V, $\bar{P}_0 = 2\ \mu\mathrm{C\,cm^{-2}}$; and in panel (d), $c_b = 10$ mM. Note that in (c), the profiles are scaled to the potential in pure water ($\kappa = 0$ Å^{-1}) at long distances, which is expressed in Eq. (86).

In Fig. 4(d), both effects of the external electrode potential and the chemisorbed water drive double layer formation, leading to an amplified electrostatic potential distribution in the solution. The inversion in the sign of the electrostatic potential at the interface seems counterintuitive at first; it appears to imply that co-ions will prefer to adsorb to a charged interface over counter-ions. Of course, as an ion approaches the interface, the surface polarization density will itself be influenced by the presence of the ion, leading to a distribution in $\tilde{P}_0$ in the plane of the interface, altering these potential profiles. Such an effect will be accounted for later in Sec. IV B.

2. Capacitance in the sharp interface model

The classical Gouy–Chapman–Stern model states the following expression for the double layer capacitance:

$$\frac{1}{C} = \frac{1}{C_{\mathrm{GC}}} + \frac{1}{C_{\mathrm{H}}}, \tag{87}$$

which arises from the separation of the electrolyte into two distinct regions, thus acting as two capacitors in series.[5] The first, concentration dependent, contribution to this capacitance, C_{GC}, comes from the diffuse double layer, which in the primitive model of the solvent is well described by Gouy–Chapman theory. The other contribution, the Helmholtz capacitance, C_{H}, is concentration independent, which could be interpreted as arising from the adsorbed Stern layer of ions. This expression can easily be validated by plotting the total inverse capacitance, $1/C$, against the inverse Gouy–Chapman capacitance, $1/C_{\mathrm{GC}}$, in a Parsons–Zobel plot.[80] For systems with no specific ion adsorption, this Parsons–Zobel plot adheres well to Gouy–Chapman–Stern theory, yielding the predicted linear relationship, with a concentration independent contribution to the capacitance, C_*. If this contribution is indeed related to C_{H}, then this plot serves as an ample validation of this picture of the double layer and the metal–solution interface.

However, despite their seemingly good agreement with Gouy–Chapman–Stern theory, these experimental results can be treated with an alternative interpretation.[81] As Fig. 4 shows, there is a potential distribution within the metal resulting from the screening behavior of the metal electrons, and so there must be a capacitance associated with it. Let us then investigate what this model predicts for the capacitance.

The differential capacitance can be calculated easily as $C = d\tilde{\sigma}/d\varphi_0$, where $\tilde{\sigma}$ is the overall charge induced in the metal by φ_0. By considering that the surface charge density must arise from an accumulation of charge over the entire metal phase, the following relationship must be true:

$$\int_{-\infty}^{0} \rho_{\mathrm{TF}} dz = \tilde{\sigma}. \tag{88}$$

Utilizing Eq. (40) and plugging in the solution for φ_{II}, the surface charge density is obtained as a function of the external voltage and surface polarization density,

$$\tilde{\sigma} = \frac{1}{4\pi}\varepsilon_{\mathrm{M}}\varkappa_{\mathrm{TF}}\left(\varphi_0 - \varphi_S(\varphi_0, \tilde{P}_0)\right). \tag{89}$$

Plotting $\tilde{\sigma}$ as a function of φ_0 for different $\tilde{P}_0$ in Fig. 5, it can clearly be seen that the potential of zero charge (pzc) shifts in the presence of chemisorbed water (as every electrochemist knows[82]), thus explaining how both effects can drive the formation of a double layer. Of course, within the linear model presented here, the differential capacitance does not depend on φ_0, and so any features, such as the Gouy–Chapman minimum or shoulders/double minima due to water structure,[14,83] will not be reproduced here. Regardless, the capacitance can be found in Eq. (89) and has two main contributions,

$$\frac{1}{C} = \underbrace{\frac{4\pi\lambda_{\mathrm{TF}}}{\varepsilon_{\mathrm{M}}}}_{1/C_{\mathrm{M}}} + \underbrace{\frac{4\pi\lambda_{\mathrm{eff,sol}}}{\varepsilon}}_{1/C_{\mathrm{sol}}}, \tag{90}$$

analogous to the Gouy–Chapman–Stern model. The first term is concentration independent, much like the Helmholtz capacitance, and the second term is the nonlocal double layer capacitance, where a new, effective characteristic length in the solution is given by

$$\lambda_{\mathrm{eff,sol}} = \frac{Q_1 Q_2 + \gamma\kappa^2}{(Q_1 + Q_2)\kappa^2}. \tag{91}$$

In the classical local electrostatic limit, i.e., $\gamma \to 1$, $\lambda_{\mathrm{eff,sol}} \to \lambda_{\mathrm{D}}$, and the classical Debye capacitance is obtained. Therefore, within this picture, the concentration independent capacitance as measured experimentally, C_*, is related to the capacitance of the metal.[84]

However, Eq. (90) has been shown in the past to completely overestimate the concentration independent inverse capacitance. Calculations using $C_*^{-1} = C_{\mathrm{M}}^{-1}$, based on the TF length of different metals, predict much larger values than experimental measurements.[81] This then presents a paradoxical problem; while it seems more physically correct to then consider a third contribution to the capacitance due to an adsorbed Stern layer of ions, where $C_*^{-1} = C_{\mathrm{H}}^{-1} + C_{\mathrm{M}}^{-1}$, such additions would worsen this overestimation.

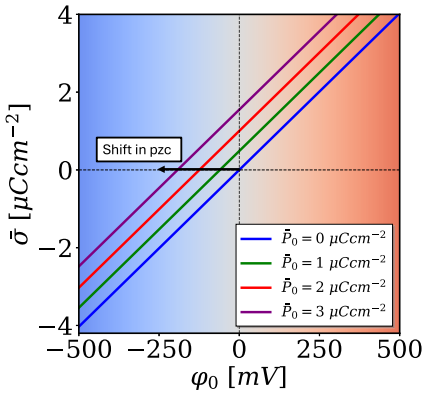

FIG. 5. Surface charge density as a function of the external electrode potential and the surface polarization density. Here, Eq. (89) is plotted with $\varepsilon = 80$, $\varepsilon_* = 5$, $\varepsilon_{\mathrm{M}} = 2$, $c_b = 10$ mM, and $\varkappa_{\mathrm{TF}} = 2$ Å^{-1}. Increasing the surface polarization density leads to a shift in the potential of zero charge.

One route taken to get around this paradox is to merely ignore this metal contribution to the capacitance. However, this is a rather displeasing solution, as it is not clear why screening in the metal should not contribute to the capacitance. Of course, the expression here was derived under the assumption that the boundary between the metal and the solution is sharp. It has instead been proposed that the interface is, in fact, diffuse, and there is interpenetration of the electrons and the solvent molecules at the interface.[85–87] Then, the electronic tails of the metal penetrate into the solvent over a distance of 1–3 Å, an effect that has been shown to bring the value of the concentration-independent contribution to the capacitance more in line with experimental results.[81,87] While such a model is strictly more accurate, in practice the sharp boundary model works reasonably well, provided the position of the boundary is shifted to account for these electron tails.[36] Thus, we will proceed in this paper with the sharp boundary model, keeping the above in mind.

B. Self-energy of a point charge at the interface

While the self-energy of a point charge was thoroughly studied above in Sec. III A, the results presented there were considered in the absence of external potential distributions imposed by the surface. To consider these effects discussed above in Sec. IV A, they must be introduced when constructing the electrostatic potential when setting up the method of images. Considering again this point-like test charge, $\varrho^{(0)}$, sitting in the electrolyte solution at $z = +a$, we, as above, introduce the two new unknown charge distributions $\tilde{\mathcal{U}}$ and $\tilde{\mathcal{V}}$ to represent the "image" charges in $\varrho_{\text{ext,I}}$ and $\varrho_{\text{ext,II}}$. However, as the two media are now nonlocal, these charges will contribute to the polarization density at the interface. Thus, if we simply linearly sum the solutions of Secs. III A and IV A and solve for $\tilde{\mathcal{U}}$ and $\tilde{\mathcal{V}}$ in the same way, then the boundary condition imposing that $P_z(z = +0) = \tilde{P}_0$ will be violated. Instead, to get around this and to solve the problem self-consistently, a new distribution, $\tilde{\mathcal{P}}$, can be introduced, representing the distribution of polarization density at the interface. This $\tilde{\mathcal{P}}$ can then be solved for and will respond to the presence of the point charge to ensure that $P_z(z = +0) = \tilde{P}_0$ is maintained. Thus, the potentials can be written in the solution as

$$\begin{aligned}\tilde{\varphi}_{\text{I}}(z,K) = {}& \frac{2\pi q}{\varepsilon}\left(\frac{g_1}{\tilde{Q}_1}e^{-\tilde{Q}_1|z-a|} + \frac{g_2}{\tilde{Q}_2}e^{-\tilde{Q}_2|z-a|}\right)\\ &+ \frac{2\pi q}{\varepsilon}\tilde{\mathcal{U}}(K)\left(\frac{g_1}{\tilde{Q}_1}e^{-\tilde{Q}_1(z+a)} + \frac{g_2}{\tilde{Q}_2}e^{-\tilde{Q}_2(z+a)}\right)\\ &+ 4\pi\left[c_1\left(\varphi_0\frac{\delta(K)}{K}, \tilde{\mathcal{P}}(K)\right)e^{-Q_1 z}\right.\\ &\left.+ c_2\left(\varphi_0\frac{\delta(K)}{K}, \tilde{\mathcal{P}}(K)\right)e^{-Q_2 z}\right],\end{aligned} \tag{92}$$

$$\begin{aligned}\tilde{\psi}_{\text{I}}(z,K) = {}& 2\pi q\left(\frac{h_1}{\tilde{Q}_1}e^{-\tilde{Q}_1|z-a|} + \frac{h_2}{\tilde{Q}_2}e^{-\tilde{Q}_2|z-a|}\right)\\ &+ 2\pi q\tilde{\mathcal{U}}(K)\left(\frac{h_1}{\tilde{Q}_1}e^{-\tilde{Q}_1(z+a)} + \frac{h_2}{\tilde{Q}_2}e^{-\tilde{Q}_2(z+a)}\right)\\ &+ 4\pi\varepsilon\kappa^2\left[\frac{1}{Q_1^2}c_1\left(\varphi_0\frac{\delta(K)}{K}, \tilde{\mathcal{P}}(K)\right)e^{-Q_1 z}\right.\\ &\left.+ \frac{1}{Q_2^2}c_2\left(\varphi_0\frac{\delta(K)}{K}, \tilde{\mathcal{P}}(K)\right)e^{-Q_2 z}\right],\end{aligned} \tag{93}$$

and in the metal as

$$\begin{aligned}\tilde{\varphi}_{\text{II}}(z,K) = {}& \frac{2\pi q}{\varepsilon_{\text{M}}}\tilde{\mathcal{V}}(K)\frac{e^{\sqrt{K^2+\varkappa_{\text{TF}}^2}(z-a)}}{\sqrt{K^2+\varkappa_{\text{TF}}^2}} + 4\pi\left[\varphi_0\frac{\delta(K)}{K}\right.\\ &\left.- \left(\varphi_0\frac{\delta(K)}{K} - \varphi_{\text{S}}\left(\varphi_0\frac{\delta(K)}{K}, \tilde{\mathcal{P}}(K)\right)\right)e^{\varkappa_{\text{TF}} z}\right],\end{aligned} \tag{94}$$

$$\begin{aligned}\tilde{\psi}_{\text{II}}(z,K) = {}& 2\pi q\tilde{\mathcal{V}}(K)\frac{e^{\sqrt{K^2+\varkappa_{\text{TF}}^2}(z-a)}}{\sqrt{K^2+\varkappa_{\text{TF}}^2}} + 4\pi\varepsilon_{\text{M}}\left[\varphi_0\frac{\delta(K)}{K}\right.\\ &\left.- \left(\varphi_0\frac{\delta(K)}{K} - \varphi_{\text{S}}\left(\varphi_0\frac{\delta(K)}{K}, \tilde{\mathcal{P}}(K)\right)\right)e^{\varkappa_{\text{TF}} z}\right].\end{aligned} \tag{95}$$

Note that here the planar geometry of the external potential contributions in each expression is maintained in the Fourier–Bessel transform by means of the factor $4\pi\delta(K)/K$. The corresponding Maxwell boundary conditions at the interface as laid out above in the Fourier–Bessel transform are written as follows:

(i) continuity of displacement field,

$$-\partial_z\tilde{\psi}_{\text{I}}(z=0,K) + \partial_z\tilde{\psi}_{\text{II}}(z=0,K) = 0, \tag{96}$$

(ii) discontinuity of potential,

$$\tilde{\varphi}_{\text{I}}(z=0,K) - \tilde{\varphi}_{\text{II}}(z=0,K) = \frac{16\pi^2\tilde{P}_0 d}{\varepsilon_*}\frac{\delta(K)}{K}, \tag{97}$$

(iii) normal component of polarization density at the interface,

$$\begin{aligned}\hat{\mathbf{n}}\cdot\mathbf{P}(z=0) &= \frac{1}{4\pi}\left(\varepsilon_*\partial_z\tilde{\varphi}_{\text{I}}(z=0,K) - \partial_z\tilde{\psi}_{\text{I}}(z=0,K)\right)\\ &= 4\pi\tilde{P}_0\frac{\delta(K)}{K}.\end{aligned} \tag{98}$$

Then, following the method of images, the distributions $\tilde{\mathcal{U}}$, $\tilde{\mathcal{V}}$, and $\tilde{\mathcal{P}}$ can be solved for, giving

$$\tilde{\mathcal{U}}(K) = \frac{\left(\frac{g_1}{\tilde{Q}_1}(\tilde{Q}_1 d - 1)e^{-\tilde{Q}_1 a} + \frac{g_2}{\tilde{Q}_2}(\tilde{Q}_2 d - 1)e^{-\tilde{Q}_2 a}\right) + \left(\frac{\xi}{\sqrt{K^2+\varkappa_{\text{TF}}^2}} - \gamma d\right)\left(h_1 e^{-\tilde{Q}_1 a} + h_2 e^{-\tilde{Q}_2 a}\right)}{\left(\frac{g_1}{\tilde{Q}_1}(\tilde{Q}_1 d + 1)e^{-\tilde{Q}_1 a} + \frac{g_2}{\tilde{Q}_2}(\tilde{Q}_2 d + 1)e^{-\tilde{Q}_2 a}\right) + \left(\frac{\xi}{\sqrt{K^2+\varkappa_{\text{TF}}^2}} - \gamma d\right)\left(h_1 e^{-\tilde{Q}_1 a} + h_2 e^{-\tilde{Q}_2 a}\right)}, \tag{99}$$

$$\tilde{\mathcal{V}}(K) = \frac{2\left(h_1 e^{-\tilde{Q}_1 a} + h_2 e^{-\tilde{Q}_2 a}\right)\left(\frac{g_1}{\tilde{Q}_1} e^{-\tilde{Q}_1 a} + \frac{g_2}{\tilde{Q}_2} e^{-\tilde{Q}_2 a}\right) e^{a\sqrt{K^2+\kappa_{\mathrm{TF}}^2}}}{\left(\frac{g_1}{\tilde{Q}_1}(\tilde{Q}_1 d+1) e^{-\tilde{Q}_1 a} + \frac{g_2}{\tilde{Q}_2}(\tilde{Q}_2 d+1) e^{-\tilde{Q}_2 a}\right) + \left(\frac{\xi}{\sqrt{K^2+\kappa_{\mathrm{TF}}^2}} - \gamma d\right)\left(h_1 e^{-\tilde{Q}_1 a} + h_2 e^{-\tilde{Q}_2 a}\right)}, \tag{100}$$

$$\tilde{\mathcal{P}}(K) = \tilde{P}_0 \frac{\delta(K)}{K} + \frac{q}{4\pi\gamma} \tilde{\mathcal{P}}_*(K), \tag{101}$$

where

$$\tilde{\mathcal{P}}_*(K) = \frac{\left(\frac{g_1}{\tilde{Q}_1} e^{-\tilde{Q}_1 a} + \frac{g_2}{\tilde{Q}_2} e^{-\tilde{Q}_2 a}\right)\left((\gamma h_1 - g_1) e^{-\tilde{Q}_1 a} + (\gamma h_2 - g_2) e^{-\tilde{Q}_2 a}\right)}{\left(\frac{g_1}{\tilde{Q}_1}(\tilde{Q}_1 d+1) e^{-\tilde{Q}_1 a} + \frac{g_2}{\tilde{Q}_2}(\tilde{Q}_2 d+1) e^{-\tilde{Q}_2 a}\right) + \left(\frac{\xi}{\sqrt{K^2+\kappa_{\mathrm{TF}}^2}} - \gamma d\right)\left(h_1 e^{-\tilde{Q}_1 a} + h_2 e^{-\tilde{Q}_2 a}\right)}. \tag{102}$$

Note here that for $d = 0$ Å, $\tilde{\mathcal{U}}(K)$ and $\tilde{\mathcal{V}}(K)$ reduce to the solutions in Eqs. (62) and (63), but the contribution from $\tilde{\mathcal{P}}$ does not disappear for $d = 0$ Å. Another important result to note is that if the charge is infinitely far away from the interface, i.e., $a \to \infty$, then $\tilde{\mathcal{P}}_*(K) \to 0$, and the electrostatic potential obtained resembles that in Sec. IV A, showing how $\tilde{\mathcal{P}}(K)$ represents the dipole layer at the interface responding to the presence of the point charge.

Interestingly, the dependence of the distributions $\tilde{\mathcal{U}}(K)$, $\tilde{\mathcal{V}}(K)$, and $\tilde{\mathcal{P}}(K)$ on the electrode potential and polarization density disappears in their calculation. This does not, however, exclude their effect from the self-energy within the image charge problem. Consider now the self-energy of the point charge in this system, as given by Eq. (5). Plugging Eq. (92) into Eq. (5) yields

$$\begin{aligned} W(a) = {} & q\left[c_1(\varphi_0, \tilde{P}_0) e^{-Q_1 a} + c_2(\varphi_0, \tilde{P}_0) e^{-Q_2 a}\right] \\ & + \frac{q^2}{2\varepsilon} \int_0^\infty KdK\ \tilde{\mathcal{U}}(K)\left(\frac{g_1}{\tilde{Q}_1} e^{-2\tilde{Q}_1 a} + \frac{g_2}{\tilde{Q}_2} e^{-2\tilde{Q}_2 a}\right) \\ & + \frac{q^2}{4\pi\gamma}\left[c_1(0,1) e^{-Q_1 a} + c_2(0,1) e^{-Q_2 a}\right] \int_0^\infty KdK\ \tilde{\mathcal{P}}_*(K), \end{aligned} \tag{103}$$

where it is clear that the first term relates to the potential distribution induced by the surface, the second term is the contribution due to the images, and the third relates to the oriented dipolar layer (originating from the adsorbed water) at the interface. Note that there is a clear difference in the expression derived in Eq. (103) compared to Eq. (64), in that there now exists a linear term in the charge of the ion, q, leading to charge-inversion asymmetry in the results. Therefore, in Secs. IV B 1 and IV B 2, results for both monovalent cations ($q = +e$) and anions ($q = -e$) are presented to highlight this.

1. Pure water limit: Effect of surface polarization

Again, it is convenient to first start with the case of pure water and not to complicate the system yet with ionic screening and the effect of an external voltage. Note that in this case, when $\kappa = 0$ Å^{-1}, there will be a non-zero constant contribution to the self-energy at long distances due to the presence of the dipole layer. Thus, the self-energy must be shifted by this constant, which takes a similar form to Eq. (86) above,

$$W(a \to \infty) = \frac{4\pi q}{\varepsilon_*} \tilde{P}_0 (\Lambda + d). \tag{104}$$

In Fig. 6(a), it can be seen straight away that the repulsive bump shown in Fig. 1 within the SRA is qualitatively reproduced here. However, this method does not quantitatively reproduce the results of the SRA for $\tilde{P}_0 = 0$ μC cm^{-2}. In allowing the surface polarization to respond to the presence of the charge, the resulting potential distribution leads to an additional repulsive contribution, shifting the adsorption minimum to positive values for $\tilde{P}_0 = 0$ μC cm^{-2}, leading to a metastable adsorbed state. There is, however, an appreciable barrier to this adsorption; if the ion can find its way to sit in this well, it would require significant energy to escape, greater than ~1 $k_B T$. Such a barrier can be thought of as a result of "interfacial de-solvation," where the presence of the ion replaces the chemisorbed water. For positively charged ions, a greater surface polarization density, and hence a stronger orientational ordering of the dipole layer, leads to a deepening of the minimum toward stable negative values, as well as the diminishing of the barrier to this adsorption. Such a result here indicates that chemisorbed water can drive the adsorption of cations at the electrochemical interface. The opposite effect is seen for anions, whereby the ordering of the interfacial dipole layer diminishes the image effects, resulting in the disappearance of the adsorption minimum.

The value taken for the short-range dielectric constant, ε_*, also has a strong effect on the self-energy profiles, plotted in Fig. 6(b). As the dielectric discontinuity gets smaller, i.e., as $\varepsilon_* \to \varepsilon_{\mathrm{M}}$, the minimum deepens significantly for both anions and cations, which can be explained in the context of the classical theory (see above). However, the barrier to this adsorption also strengthens, as the repulsive contribution due to the polarization density is greater as the "background permittivity" decreases.

As was made clear from the analysis in Sec. III, the properties of the metal can influence the self-energy profile. We plot results in varying the TF screening length in the metal in Fig. 6(c).

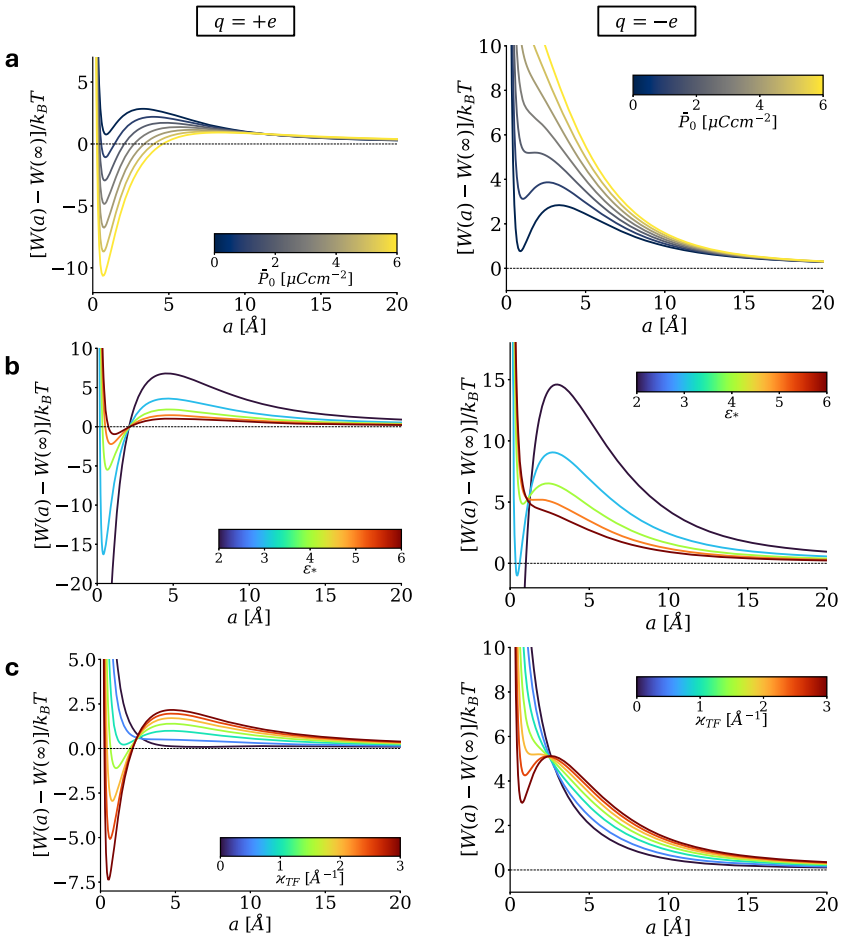

FIG. 6. Self-energy profiles of a point charge at the metal/pure water interface, accounting for surface polarization at the interface. The left column is plotted for positively charged, monovalent cations ($q = +e$); and the right column is plotted for negatively charged, monovalent anions ($q = -e$). (a) Self-energy for a charge from Eq. (103) for different $\bar{P}_0$, representing the strength of ordering of the dipole layer. Unless otherwise stated, in all plots, for the TF metal, parameters used are $\varepsilon_M = 2$ and $\varkappa_{TF} = 2$ Å^{-1}; and for the nonlocal Lorentzian model, parameters used are $\varepsilon = 80$, $\varepsilon_* = 5$, and $\Lambda = 3$ Å. (b) Dependence of the self-energy on the short-range dielectric constant, ε_*. Values of ε_* can range from 2 to 6, indicated by the color bar. (c) Dependence of the self-energy on the TF screening length. Values of $\varkappa_{TF}$ range from 0 to 3 Å^{-1}, indicated by the color bar. In panels (b) and (c), $\bar{P}_0 = 2$ μC cm^{-2}.

For $\varkappa_{TF} \to 0$ Å^{-1}, i.e., the metal side representing a dielectric, the ion is repelled from the interface, again because $\varepsilon_* > \varepsilon_M$. However, just like above, as $\varkappa_{TF}$ increases and the screening length decreases, the metal becomes a better conductor, and so the minimum deepens as the field generated by the charge gets more quickly screened within the metal. However, a new effect emerges here (formally, because this is not something that we can easily vary in the metal); the barrier to adsorption gets larger with decreasing screening length. The origin of such an effect can be attributed to the degree to which the dipole layer responds to the presence of the ion.

2. Effect of applied voltage

For a positively charged ion, applying a negative external electrode potential introduces a longer-ranged attractive tail to the self-energy. The range of this tail depends on the electrolyte concentration, which can be clearly seen between Figs. 7(a) and 7(b), as the electrolyte ions screen the charge of the electrode. In all cases, a strong minimum due to the image contribution to the self-energy appears in the vicinity of the interface. However, if too close to the interface, the effect of the field of the point charge penetrating into the metal will always yield a strong repulsive force, provided $\varepsilon_*/\varepsilon_M > 1$. This explains why, even at strongly positive (repulsive) surface potentials, the self-energy still exhibits a metastable minimum, which could explain the phenomenon of underpotential deposition (UPD) (see Sec. VI below).

The more interesting case is when voltages opposite to the charge of the ion are applied. Of course, further away from the interface, a positively charged ion is repelled by a positively charged electrode. However, for small to intermediate applied voltages, there is an energy barrier leading to an adsorption minimum close to the interface, arising from the interplay between the electrode potential, the nonlocal dielectric response of the solvent, and the ability for the field to penetrate the metal. This barrier is reasonable for lower background electrolyte concentrations, showing the possibility of ions becoming trapped close to the electrode. Of course, as the applied voltage is driven to greater values, or for higher concentrations, this effect diminishes, and the point charge is then repelled from the interface.

Note that these effects discussed above depend strongly on ε_*. In all plots, ε_* is taken to be 5. However, it is currently unknown what value this parameter should take. For example, if this short-range dielectric constant encapsulates the electronic polarizability

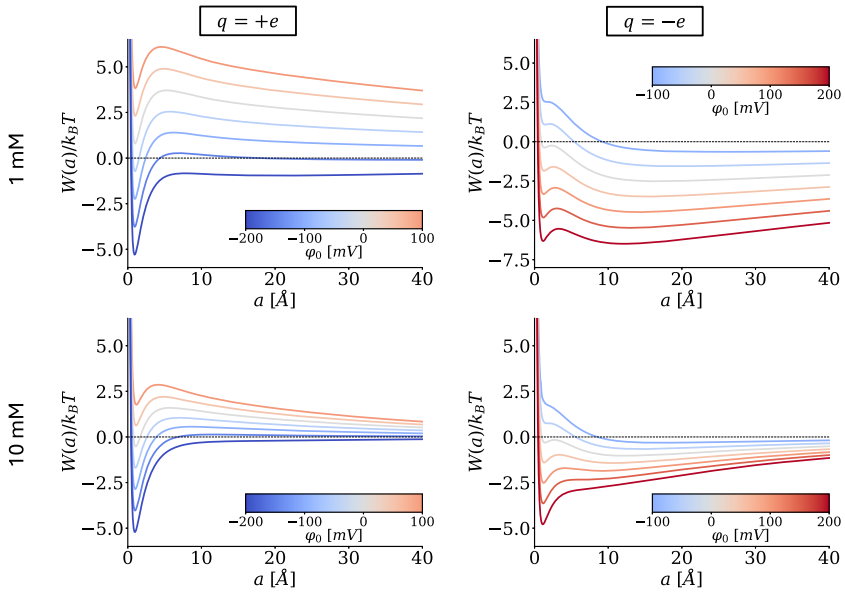

FIG. 7. Dependence of the self-energy on the applied voltage. Self-energy profiles calculated by means of Eq. (103). Here, $\varepsilon = 80$, $\varepsilon_* = 5$, $\varepsilon_M = 2$, $\varkappa_{TF} = 2$ Å^{-1}, and $\Lambda = 3$ Å. The surface polarization density is taken to be $\tilde{P}_0 = 2\ \mu$C cm^{-2}. Here, the rows correspond to the two different electrolyte concentrations, $c_b = 1$ mM (top) and $c_b = 10$ mM (bottom). The columns indicate the sign of the charge, with the left for positively charged monovalent cations ($q = +e$) and the right for negatively charged monovalent anions ($q = -e$). The effect of varying an applied voltage on the self-energy profiles is indicated by the color scales in each plot.

of water, then $\varepsilon_* = 1.98$. Otherwise, if it describes vibrational and infrared polarization modes, then it can range between 3 and 5. However, one could also argue that ε_* should just be 1, the vacuum limit. Thus, what is presented here is the weakest effect possible within this framework, as when ε_* decreases, the adsorption minimum strengthens. Thus, it can be used as a tunable parameter in comparisons against experimental results.

Similar results have been calculated in the past in Ref. 23 for the self-energy of an ion at the TF metal/nonlocal electrolyte interface within the SRA, showing this non-monotonic behavior. However, while the origin of this behavior was attributed to bound surface charge, this was cumbersome to derive, and the formulation did not allow for understanding how interfacial water structure may contribute to driving the adsorption of ions. Through the field-theoretic approach used throughout the paper, the origins of these effects are clearer and do not rely on any approximation of the dielectric function at the interface.

V. ELECTROSTATIC POTENTIAL CREATED BY AN ION AT THE INTERFACE

A. Field penetration in the metal

The concept of the electric field of the point charge penetrating into the metal has been mentioned several times throughout this paper so far; let us now clarify what is meant by this. Consider the classical model for a perfect conductor; with a dielectric constant tending to infinite values, the electric field, and hence the charge density within the metal, is zero. Thus, due to the continuity of potential, the field at the interface is also zero, as the electrons in the metal are able to perfectly screen the field created by the point charge, leading to the attractive classical self-energy law derived above. Thus, there is no penetration of the field into the ideal metal conductor.

This is, of course, not the case for the TF metal. Electrons screen the field over the TF length; thus, if the point charge is too close to the interface such that the electrons are not able to sufficiently screen the field it creates, it feels a repulsive force, as the point charge begins to see the positively charged background skeleton of the metal. This effect can be seen explicitly by calculating the potential in all space.

The electrostatic potential in real space can be written by inserting Eqs. (92) and (94) into Eq. (5.43), yielding in the electrolyte solution,

$$\begin{aligned}\varphi_{\mathrm{I}}^{z\geq 0}(z,R) = {}& \left[c_1(\varphi_0,\tilde{P}_0)e^{-Q_1 z} + c_2(\varphi_0,\tilde{P}_0)e^{-Q_2 z}\right] + \frac{q}{\varepsilon\sqrt{R^2+(z-a)^2}} \\ & \times \left(g_1 e^{-Q_1\sqrt{R^2+(z-a)^2}} + g_2 e^{-Q_2\sqrt{R^2+(z-a)^2}}\right) \\ & + \frac{q}{2\pi\gamma}\left[c_1(0,1)e^{-Q_1 z} + c_2(0,1)e^{-Q_2 z}\right] \\ & \times \int_0^\infty K J_0(KR)\tilde{\mathcal{P}}_*(K)dK + \frac{q}{\varepsilon}\int_0^\infty KdK\ J_0(KR)\tilde{\mathcal{U}}(K) \\ & \times \left(\frac{g_1}{\tilde{Q}_1}e^{-\tilde{Q}_1(z+a)} + \frac{g_2}{\tilde{Q}_2}e^{-\tilde{Q}_2(z+a)}\right),\end{aligned} \tag{105}$$

and in the metal,

$$\begin{aligned}\varphi_{\mathrm{II}}^{z<0}(z,R) = {}& \left[\varphi_0 - \left(\varphi_0 - \varphi_S(\varphi_0,\tilde{P}_0)\right)e^{\varkappa_{\mathrm{TF}} z}\right] \\ & + \frac{q}{2\pi\gamma}\varphi_S(0,1)e^{\varkappa_{\mathrm{TF}} z}\int_0^\infty K J_0(KR)\tilde{\mathcal{P}}_*(K)dK \\ & + \frac{q}{\varepsilon_{\mathrm{M}}}\int_0^\infty KdK\ J_0(KR)\tilde{\mathcal{V}}(K)\frac{e^{\sqrt{K^2+\varkappa_{\mathrm{TF}}^2}}}{\sqrt{K^2+\varkappa_{\mathrm{TF}}^2}},\end{aligned} \tag{106}$$

where in Eq. (105), the second term represents the potential created by the point charge in the bulk of the aqueous solution. For simplicity, let us first consider the interface in the absence of an

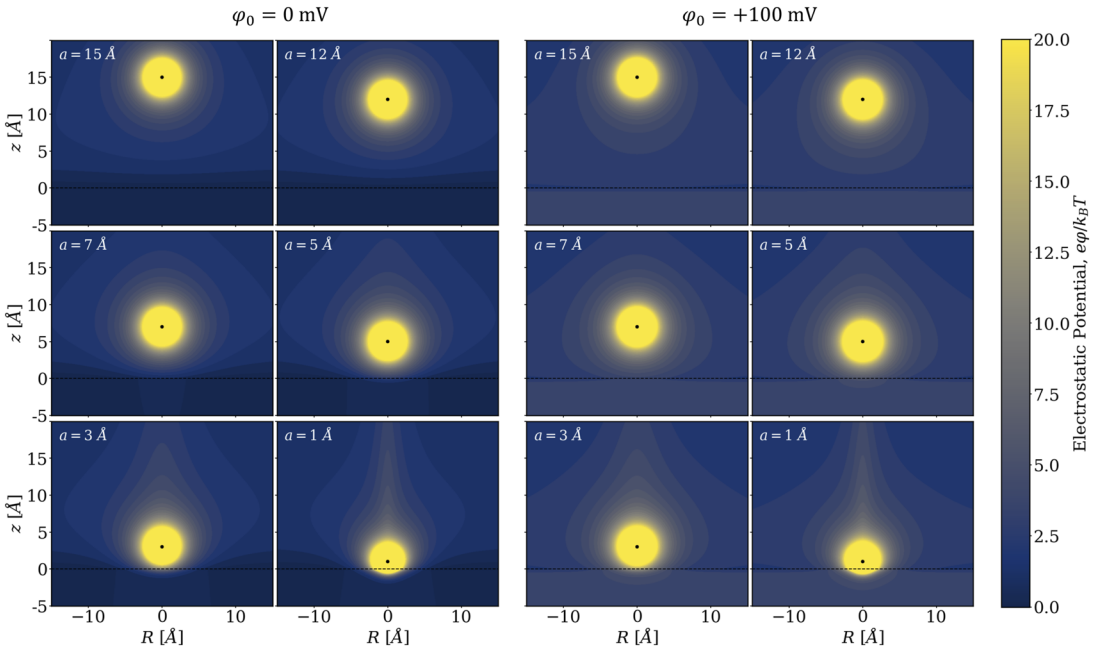

FIG. 8. Electrostatic potential distribution at the metal/solution interface. Contour maps of the potential distribution as plotted from Eqs. (105) and (106), for $\varphi_0 = 0$ mV (left) and $\varphi_0 = 100$ mV (right). In all plots, the interface at $z = 0$ is depicted by a dashed black line. The black circle indicates the position of the point charge, and its distance from the interface, a, is indicated in each plot. Parameters for the metal were $\varepsilon_M = 2$ and $\varkappa_{TF} = 2$ Å^{-1}; and in the solution, $c_b = 10$ mM, $\varepsilon = 80$, $\varepsilon_* = 5$, and $\Lambda = 3$ Å; and $\bar{P}_0 = 2$ μC cm^{-2}.

applied voltage, i.e., $\varphi_0 = 0$ mV. The electrostatic potential distribution as the point charge approaches the interface is plotted in Fig. 8 (left). There are a few key observations to note here. When the charge is further away from the electrode, the planar wave of potential generated by the chemisorbed dipoles at the interface distorts the field created by the point charge, resulting in the repulsive barrier in the self-energy. However, when the charge is moved closer to the interface, this planar wave distorts, leaving a "cavity" in which the charge can begin to "feel" the metal. It is at this point where the field created by the charge begins to penetrate the metal, where it is rapidly screened by the metal electrons, leading to the adsorption minimum in the self-energy. This results in a "pancake"-like, thin layer of electrons close to the interface. As the charge approaches even closer, this "pancake" becomes more bell-shaped, and the electronic density becomes insufficient to screen the charge at the interface. Here, the charge is then able to feel the positively charged skeleton of the metal ion cores and is strongly repelled.

Looking in the lateral (R-) direction to the charge, parallel to the interface, the field contracts, being screened more strongly with the characteristic lengths depending on the properties of both the contacting media. This kind of effect is known,[21,22] and it can have important consequences on the adsorption of ions at the electrochemical interface[47,88] and will be examined in detail in Subsection V B.

Then, applying a repulsive voltage across the system, the field of the ion is distorted more strongly at a longer range, directly relating to its stronger repulsion from the interface. As the charge approaches the interface, the planar wave of potential arising from the surface polarization deforms again, and the field of the ion penetrates the metal. The origin of the adsorption minimum, even at repulsive applied voltages, is thus made clear.

Of course, here the sharp interface approximation was used, constraining the electrons to sit only at $z < 0$. If a diffuse interface were modeled here instead, as the charge approaches the interface, the "pancake" of electrons would be expected to extrude out from the metal skeleton into the solution bulk, as they are pulled toward the charge source. A similar effect would be expected under the influence of an applied voltage.[87]

B. Lateral interaction of charges at the interface

So far in this paper, it has been established how a single point charge may behave at the interface between a TF metal and a nonlocal aqueous solution. In reality, there will be many more than just single charges at the interface, and so their interaction in the plane of adsorbed ions, i.e., at $z = a$, must be considered. For point charges, in the linear response approximation considered so far across the paper, this will simply be proportional to the electrostatic potential, as previously calculated, and so, the lateral potential profile will be of interest here. Although having previously been extensively studied within a local picture of water,[27,47,89] such a problem is gathering renewed interest, with more recent theoretical[76] and computational[77] advances supporting these classical results, but in

TABLE I. Limiting laws for the electrostatic potential. Approximate limiting laws for the lateral electrostatic potential at the TF–dielectric interface (middle) and at the conductor–dielectric interface (right) for the indicated parameter regimes, as presented in Ref. 89.

	Parameter regime	Limiting laws	Classical ($\varkappa_{\mathrm{TF}} \to \infty$)
(1)	$a \approx R \ll \xi\varkappa_{\mathrm{TF}}^{-1}$	$\frac{q}{\varepsilon}\left\{\frac{1}{R} + \left(\frac{\xi-1}{\xi+1}\frac{1}{\sqrt{R^2+4a^2}}\right)\right\}$	$\frac{q}{\varepsilon}\left\{\frac{1}{R} - \frac{1}{\sqrt{R^2+4a^2}}\right\}$
(2)	$a \ll R \ll \xi\varkappa_{\mathrm{TF}}^{-1}$	$\frac{q}{\varepsilon}\left\{\frac{2\xi}{\xi+1}\right\}\frac{1}{R}$	$\frac{q}{\varepsilon}\left\{\frac{2a^2}{R^3}\right\}$
(3)	$a \le \xi\varkappa_{\mathrm{TF}}^{-1} \ll R$	$\frac{q}{\varepsilon}\left\{\frac{2(a+\xi\varkappa_{\mathrm{TF}}^{-1})^2}{R^3}\right\}$	$\frac{q}{\varepsilon}\left\{\frac{2a^2}{R^3}\right\}$

these works the medium in contact with the TF metal was still considered to be local. Thus, there is a strong impetus to see how the nonlocal theory developed here compares with those established results.

Before proceeding to the fully nonlocal formulation, let us first consider how just a TF metal can distort the field created by an ion, looking back to the work in the 1980s.[22,27,47,89] In Table I, limiting laws of the lateral potential are presented in the middle column for a local water–TF interface, describing how the charges may interact in the plane of such an interface,[89] approximated at different ranges of separation, R. For comparison, the classical laws for an ideal metal are also shown in the right-hand column. It can be seen from these limiting laws that, when penetration of the ion field into the metal is permitted, there arises a rather dramatic enhancement of the field in comparison to the classical model. Such an effect occurs as a direct consequence of this "pancake" of charge induced in the metal, as shown above in Sec. V A. However, this demonstrates that the repulsive lateral interaction between charges of the same sign is stronger than the classical model predicts at the metal–water interface, thereby discouraging ions from packing closely at the surface.

Intuitively, such a result does not bode well for a nonlocal electrostatic model. If the dielectric constant is dramatically reduced in the vicinity of the point charge, the lateral field would be enhanced greatly, further discouraging the adsorption of ions at the interface. For a more direct comparison with Table 5.1, let us first consider now a similar case in the field theoretical approach, using the result from Sec. III B neglecting surface polarization and applied voltage effects. In the absence of background electrolyte ($\kappa = 0$), the lateral interaction potential in the plane of the point charge ($z = a$) reads as

$$\begin{aligned} u_{\parallel}(a,R) &= \varphi_{\mathrm{I}}(z=a,R;\kappa=0) - \varphi_{\mathrm{II}}(z=a,R\to\infty;\kappa=0) \\ &= \frac{q}{\varepsilon R}\left(1+(\gamma-1)e^{-R/\Lambda}\right) + \frac{q}{\varepsilon}\int_0^\infty dK\, J_0(KR)\mathcal{U}_{\mathrm{pure}}(K) \\ &\quad\times\left(e^{-2Ka} + \frac{K(\gamma-1)}{\sqrt{K^2+1/\Lambda^2}}e^{-2a\sqrt{K^2+1/\Lambda^2}}\right), \end{aligned} \tag{107}$$

where $\mathcal{U}_{\mathrm{pure}}(K)$ is given in Eq. (66). This potential is plotted as a function of R in Fig. 9 and compared against the laws in Table I. In all cases, there is a clear enhancement of the field when considering the TF model of the metal in comparison to the classical, ideal conductor model. As mentioned above, this is a direct consequence of the penetration of the field into the metal and is an expected result here.[22,27,47,89] The local limit of the theory (red curve in Fig. 9), where $\gamma = 1$, adheres well to the limiting laws (1) and (3), representing the behavior close to and far away from the charge along the interface. Limiting law (2), however, seems to dramatically overestimate the field at intermediate ranges. One can note that (1) reduces to (2) in the case when $a \to 0$ Å, indicating that (2) is only valid when the charge is directly at the interface. This may mean much more favorable results for ion adsorption, as the repulsion between charges at the interface is dramatically reduced at intermediate separations compared to those previous estimates.

Now considering the nonlocal theory of the water [blue curve in Fig. 9(a)], at close distances to the point charge, the field is very strongly enhanced, a consequence of the reduced effective dielectric constant in this regime. However, at intermediate and larger separations, there is a crossover between the nonlocal and local limits, where the nonlocal theory reveals a much more diminished repulsion than expected, likely a result of the enhanced, coupled electron and dipole screening effects from the TF and Lorentzian models used. Although not shown here, plotting similar curves for the full model accounting for the background electrolyte concentration only slightly increases this screening effect, diminishing the repulsive lateral interaction further. Such a finding is, in fact, more beneficial for the picture of adsorption, as a reduced repulsion between charges can lead to denser lattices of ions at the interface; this will be explored in Sec. VI.

In the Appendix, we compared the SRA-based old results of Ref. 22 for the electrostatic potential created by the charge with our field-theoretical approach. The results are qualitatively similar, but in the absence of surface polarization, they become identical when the charge sits right at the boundary between the metal and electrolyte. The Appendix also contains numerical testing of all the asymptotic laws coming from the formulas obtained in Ref. 22, which surprisingly has not been done in the past. The tests approve all laws listed above in Table I, but they indicate that the asymptotic law for the short distances from the charge, when it is near the interface, is reproduced only at very short distances.

To go further, let us now consider the more complete theory presented in Sec. IV. Accounting for surface effects, the lateral interaction potential is given by

$$\begin{aligned} u_{\parallel}(a,R) &= \frac{q}{\varepsilon R}\left(g_1 e^{-Q_1 R} + g_2 e^{-Q_2 R}\right) + \frac{q}{\varepsilon}\int_0^\infty KdK\, J_0(KR)\tilde{\mathcal{U}}(K) \\ &\quad\times\left(\frac{g_1}{\tilde{Q}_1}e^{-2\tilde{Q}_1 a} + \frac{g_2}{\tilde{Q}_2}e^{-2\tilde{Q}_2 a}\right) \\ &\quad+ \frac{q}{2\pi\gamma}\left[c_1(0,1)e^{-Q_1 a} + c_2(0,1)e^{-Q_2 a}\right] \\ &\quad\times\int_0^\infty KdK\, J_0(KR)\tilde{\mathcal{P}}_*(K). \end{aligned} \tag{108}$$

Note that the explicit effect of the applied voltage and surface polarization density disappears from this expression, as it simply behaves as a constant value in the interaction. However, not all effects are removed; the response of the interfacial dipole layer through $\tilde{\mathcal{P}}_*(K)$ to the point charge remains in the third term in Eq. (108).

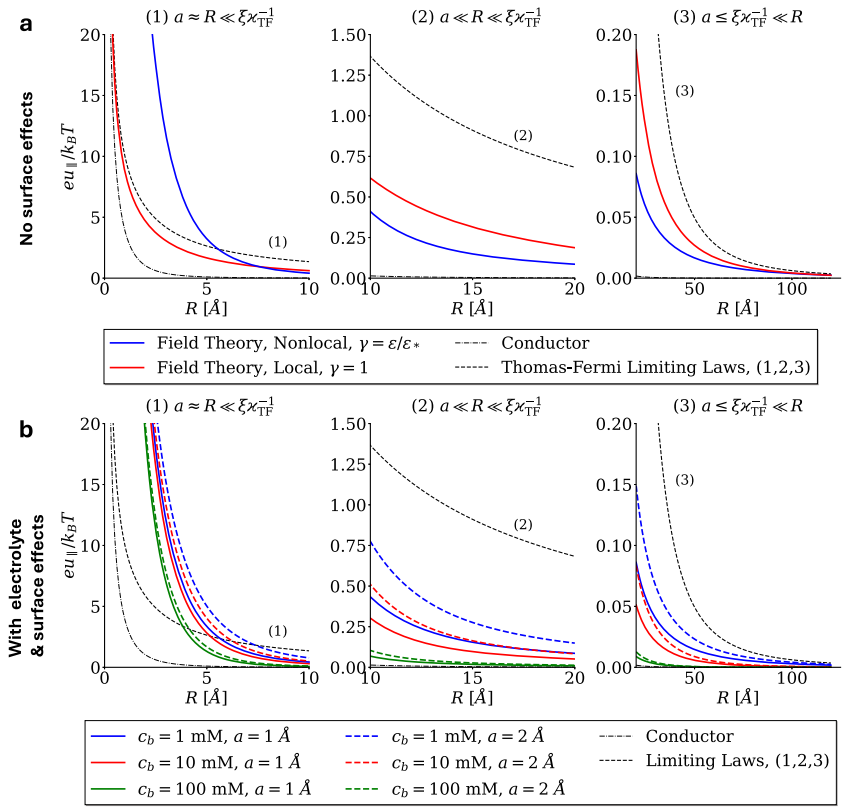

FIG. 9. Lateral dependence of the electrostatic potential in the plane of the point charge. Comparison between the results of (a) Eq. (107) and (b) Eq. (108) with the indicated limiting laws in Table 5.1. The middle and right columns of Table 5.1 are given by dashed and dotted-dashed lines, respectively. For all plots, $\varepsilon_M = 2$, $\varkappa_{TF} = 2$ Å^{-1}, $\varepsilon = 80$, $\varepsilon_* = 5$, and $\Lambda = 3$ Å; and in panel (b), $\bar{P}_0 = 2$ μC cm^{-2}. In panel (a), the blue and red curves indicate the nonlocal and local ($\gamma = 1$) limits of the theory, respectively. In panel (b), the colors represent the different bulk electrolyte concentrations, showing the screening of the lateral potential. The solid and dashed colored lines in panel (b) show results for $a = 1$ Å and $a = 2$ Å, respectively.

Plotting Eq. (108) against the limiting laws in Fig. 9(b) shows a similar behavior for the nonlocal theory in the absence of surface effects and electrolyte screening. At short distances, the interaction potential is enhanced due to nonlocal Lorentzian correlations in the water. However, this also leads to enhanced screening, thus resulting in a crossover between the nonlocal and local laws, with the longer-range behavior showing a dramatically reduced repulsive interaction. Of course, as the bulk electrolyte concentration increases, the screening of the potential is also enhanced, leading to an overall reduced repulsive lateral interaction.

The effect of field penetration into the metal is made clearer when comparing the lateral interaction potential distribution created by the ion located at different distances from the surface; in Fig. 9, curves are plotted for both $a = 1$ Å and $a = 2$ Å. Simply bringing the point charge closer to the interface spreads the radius of the "pancake" of charge formed in the metal, which screens the lateral potential distribution, thereby reducing the repulsion in the lateral plane.

In both Figs. 9(a) and 9(b), at long distances, past the range of polarization fluctuation and electron correlation effects, all the profiles converge. Of course, within such a simple Lorentzian model, no complicated effects of overscreening can occur. Those effects, however, would have resulted in a series of deep, attractive minima between the charges at close separations. Similarly, this TF model neglects more complicated oscillatory behavior in the metal, which could be introduced through the more general Lindhard model.[22,52] This model, however, is at least a first step to understanding more deeply the role water may play at the electrochemical interface.

VI. ADSORPTION AT THE ELECTROCHEMICAL INTERFACE

Now with a fuller picture of the electrostatics at play within this model, it seems natural to explore their physical consequences, and in particular, their effect on ion adsorption. As shown above in Sec. IV, applying a negative electrode potential will naturally draw charges toward the interface. However, only the case of one charge was considered there. Consider a 2D grid in the plane of the interface; if each site within the grid were to be occupied by a charge, then charges in neighboring sites would interact repulsively in the plane of the interface, with the lateral potential studied in Sec. V B describing these forces. There are then two competing contributions at play when considering multiple charges" the self-energy and the pair interaction.

Then, let us now attempt to build a model of ion adsorption at the electrochemical interface, accounting for ion–image and ion–ion interactions. To begin with, let us consider the entropic contribution to the chemical potential, μ_{ent}, within a lattice gas approximation. To do this, we must separate the system into two sub-systems, the "adsorbed" lattice sites of the metal (N_s) and the non-adsorbed "solution" sites (N_{sol}). Then, we consider N ions distributed across

all these sites, with a certain portion, N_{ads}, adsorbed to the metal, such that $N - N_{ads}$ ions remain in the solution. Considering all this, the total number of combinations can be written as

$$\Omega = \frac{(N_s + N_{sol})!}{N_a!(N_s - N_a)!(N - N_a)!(N_{sol} - N + N_a)!}. \tag{109}$$

Then, considering the entropy of mixing is given by $S = k_B \ln \Omega$, and using Stirling's approximation ($\ln x! \approx x \ln x - x$ for $x \gg 1$), the entropic contribution to the chemical potential of adsorbed ions is given by

$$\frac{\mu_{ent}}{k_B T} = \frac{\partial(-TS)}{\partial N_{ads}} \approx \ln\left[\frac{N_{ads}(N_{sol} - N + N_{ads})}{(N - N_{ads})(N_s - N_{ads})}\right]. \tag{110}$$

If we assume that the number of ions adsorbing to the surface is much smaller than the total number of ions (i.e., $N_{ads} \ll N$), and also that the number of unadsorbed ions is much smaller than the number of available sites in the solution (i.e., $N - N_{ads} \ll N_{sol}$), then the following approximation can be made:

$$\ln\left[\frac{N_{ads}(N_{sol} - (N - N_{ads}))}{(N - N_{ads})(N_s - N_{ads})}\right] \approx \ln\left[\frac{N_{ads} N_{sol}}{N(N_s - N_{ads})}\right] = \ln\left[\frac{N_{ads}}{N_s - N_{ads}}\right] - \ln\left[\frac{N}{N_{sol}}\right]. \tag{111}$$

Defining the surface coverage, $\theta = N_{ads}/N_s$, and the bulk concentration of the specifically adsorbing ions as $\tilde{c} = N/N_A V$, where N_A is Avogadro's constant and V is the volume of the solution, this can be written as

$$\frac{\mu_{ext}}{k_B T} = \ln\left[\frac{\theta}{1-\theta}\right] - \ln\left[\tilde{c} N_A V_{ads}\right], \tag{112}$$

where V_{ads} is the volume of a site in the solution, which we can approximate to be that of a hydrated ion. The first term in Eq. (111) represents the entropic contribution of the chemical potential in the adsorbed state, $\mu_{ent,ads}$, and the second term is the bulk chemical potential, μ_{bulk}. With the entropic contribution defined, we now consider the "external" chemical potential of the adsorbed state, which contains all electrostatic terms above,

$$\frac{\mu_{ext,\,ads}}{k_B T} = \frac{W}{k_B T} + \frac{W^*}{k_B T} + \frac{e\tilde{u}_\parallel}{k_B T}\theta, \tag{113}$$

where $W \equiv W(a; \varphi_0, \tilde{P}_0)$ is the self-energy of the adsorbing point charge, as given by Eq. (103), and $-W^* \approx 4$–$5 k_B T$ defines an additional attraction energy, which is assigned to a possible chemical bonding of the ion to the interface, not considered above. Given the slowness of the decay of the potential in the lateral plane of the interface, it is not possible to limit the in-plane interactions to nearest-neighbors. Instead, we define the mean lateral interaction potential, $\tilde{u}_\parallel$, as an average potential created by all other ions adsorbed on the surface. For our purposes, we utilize the "cut-out disk" approximation.[47] Here, the given particle is assumed to sit in a circle of radius r_c, with no other particles inside, but with a uniform constant surface density of ions, c_s, sitting outside this circle. Thus, this mean interaction potential is defined as

$$\tilde{u}_\parallel(a, \theta) = 2\pi c_s(\theta) \int_{r_c(\theta)}^{\infty} R dR\, u_\parallel(a, R), \tag{114}$$

where we can write $c_s = \theta/(\pi r_{ads}^2)$, and $r_{ads} \approx 3$–5 Å is the hydrated radius of the adsorbing ion. Note that here, the radius r_c is also a function of the surface coverage and can be defined as

$$r_c(\theta) = \frac{1}{\sqrt{\pi c_s(\theta)}} = \frac{r_{ads}}{\sqrt{\theta}}. \tag{115}$$

Plugging Eq. (108) into Eq. (114) and using the Bessel function identity,

$$J_0(KR) = \frac{1}{KR}\frac{\partial}{\partial K}[K\, J_1(KR)],$$

we obtain

$$\begin{aligned}\tilde{u}_\parallel(a, \theta) = {} & \frac{2\theta}{r_{ads}^2}\frac{q}{\varepsilon}\left(\frac{g_1}{Q_1}e^{-Q_1\left(r_{ads}/\sqrt{\theta}\right)} + \frac{g_2}{Q_2}e^{-Q_2\left(r_{ads}/\sqrt{\theta}\right)}\right) \\ & - \frac{\sqrt{\theta}}{\pi r_{ads}}\frac{q}{\gamma}\left[c_1(0,1)e^{-Q_1 a} + c_2(0,1)e^{-Q_2 a}\right] \\ & \times \int_0^\infty dK\, J_1\left(\frac{K r_{ads}}{\sqrt{\theta}}\right)\tilde{\mathcal{P}}_*(K) \\ & - \frac{2\sqrt{\theta}}{r_{ads}}\frac{q}{\varepsilon}\int_0^\infty dK\, J_1\left(\frac{K r_{ads}}{\sqrt{\theta}}\right)\tilde{\mathcal{U}}(K) \\ & \times \left(\frac{g_1}{\tilde{Q}_1}e^{-2\tilde{Q}_1 a} + \frac{g_2}{\tilde{Q}_2}e^{-2\tilde{Q}_2 a}\right).\end{aligned} \tag{116}$$

Under equilibrium conditions, we can equate the total chemical potential, $\mu_{ext,ads} + \mu_{ent,ads}$, with the bulk chemical potential, μ_{bulk}, yielding a general adsorption isotherm,

$$\frac{W(a; \varphi_0, \tilde{P}_0)}{k_B T} + \frac{W^*}{k_B T} + \frac{e\tilde{u}_\parallel(a, \theta)}{k_B T}\theta + \ln\left[\frac{\theta}{1-\theta}\right] - \ln\left[\tilde{c} N_A V_{ads}\right] = 0. \tag{117}$$

From this, we can calculate the dependence of the surface coverage with two main parameters of interest: (i) the external electrode potential, φ_0; and (ii) the bulk concentration of adsorbing ions, $\tilde{c}$.

To find the coverage as a function of the external potential, let us first extract the term responsible for the φ_0-dependence in the general isotherm. Taking the first term of Eq. (117) and using Eq. (103), the image contribution to the isotherm can be broken down as

$$\frac{W(a; \varphi_0, \tilde{P}_0)}{k_B T} = \frac{W_1(a; \varphi_0)}{k_B T} + \frac{W_2(a; \tilde{P}_0)}{k_B T}, \tag{118}$$

where the two terms can be written as

$$\frac{W_1(a; \varphi_0)}{k_B T} = \frac{e\varphi_0}{k_B T}\left[c_1^{(1)}e^{-Q_1 a} + c_2^{(1)}e^{-Q_2 a}\right], \tag{119}$$

and

$$\begin{aligned}\frac{W_2(a; \tilde{P}_0)}{k_B T} = {} & \frac{4\pi\gamma\ell_B\tilde{P}_0}{e}\left[c_1^{(2)}e^{-Q_1 a} + c_2^{(2)}e^{-Q_2 a}\right] \\ & + \ell_B\left[c_1^{(2)}e^{-Q_1 a} + c_2^{(2)}e^{-Q_2 a}\right]\int_0^\infty K\tilde{\mathcal{P}}_*(K)dK \\ & + \frac{\ell_B}{2}\int_0^\infty KdK\, \tilde{\mathcal{U}}(K)\left(\frac{g_1}{\tilde{Q}_1}e^{-2\tilde{Q}_1 a} + \frac{g_2}{\tilde{Q}_2}e^{-2\tilde{Q}_2 a}\right),\end{aligned} \tag{120}$$

where the coefficients are defined in terms of Eqs. (83) and (84),

$$c_1^{(1)} = c_1(1,0), \quad c_1^{(2)} = \frac{\varepsilon*}{4\pi} c_1(0,1),$$
$$c_2^{(1)} = c_2(1,0), \quad c_2^{(2)} = \frac{\varepsilon*}{4\pi} c_2(0,1).$$

This enables a straightforward way to explicitly obtain the electrosorption isotherm,

$$\frac{e\varphi_0(\theta)}{k_BT} = \frac{1}{c_1^{(1)}e^{-Q_1 a} + c_2^{(1)}e^{-Q_2 a}} \left\{ \ln\left[\tilde{c}N_A V_{\text{ads}}\right] + \ln\left[\frac{1-\theta}{\theta}\right] - \frac{W_2(a;\tilde{P}_0)}{k_BT} - \frac{W^*}{k_BT} - \frac{e\tilde{u}_{\parallel}(a,\theta)}{k_BT}\theta \right\}. \quad (121)$$

The adsorption isotherm we came to contains W^* as one of the main driving forces for the possibility of underpotential deposition (UPD) of ions (see Refs. 90 and 91). W^* describes specific interactions between the ions under study and the metal surfaces. It is different for different metal–ion combinations, such as copper, silver, lead, and mercury ions on gold; copper and silver ions on platinum; and lead and thallium on silver, etc.[92] Below we explore other factors affecting the adsorption, such as electrostatic interactions between the ion and electrode and between the adsorbed ions, both affected by water structure and electric field penetration into the metal. Thus, as a disclaimer, when trying to demonstrate how the change of those factors in a series of metals will affect UPD, we cannot describe the whole UPD phenomenon unless we simultaneously vary W^* for every metal-ion combination.

Electrosorption isotherms: The isotherms described by Eq. (121) are plotted in Fig. 10 for positively charged ions, i.e., $q = +e$. It is clear, looking at all of the curves, that the isotherms are sensitive to the balance between the attractive self-energy and the repulsive lateral interaction energy contributions. Note that the isotherms have been plotted within the electrochemical window; outside of this range, reductive and oxidative electron transfer processes may occur, which are not accounted for in this model. To explore different effects on electrosorption isotherms, we have varied the following parameters.

In Fig. 10(a), the hydrated radius of the adsorbing ions, r_{ads}, is varied, which is directly related to the density of the adsorbing layer, where smaller r_{ads} indicates a denser lattice. As the charges are packed more densely on the electrode, and thus also with an increase in the coverage, θ, the repulsive lateral interaction contribution becomes stronger, resulting in the isotherm flattening out. Thus, much greater negative voltages are required to achieve the same coverage.

The importance of the entropic contribution to the electrosorption isotherm is shown in Fig. 10(b). Increasing the bulk concentration of the adsorbing ions, $\tilde{c}$, provides an entropic drive for the ions to adsorb to the interface from the bulk, leading to a shift in the isotherm to more positive potentials. This can be seen more clearly in Fig. 11 and is discussed below.

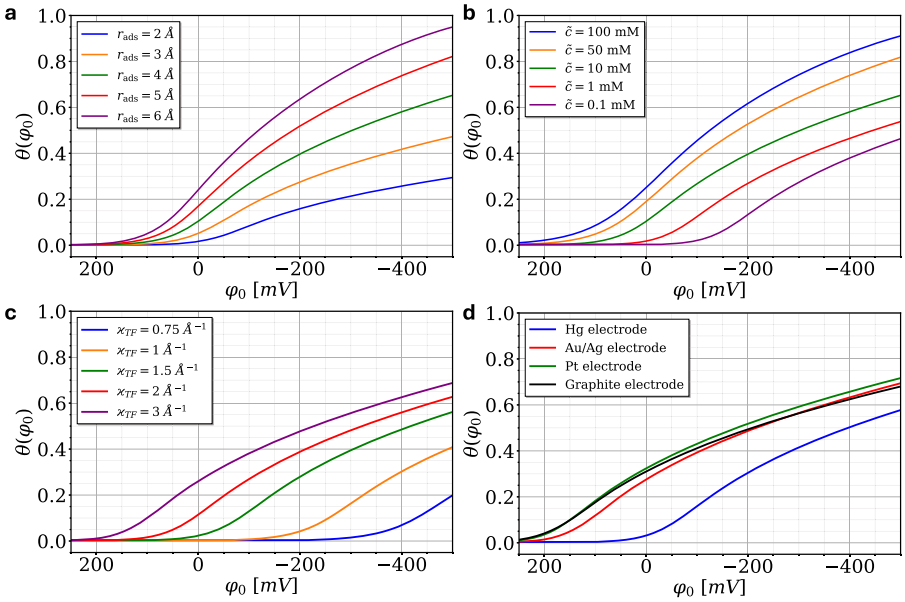

FIG. 10. Electrosorption isotherms at the TF metal–nonlocal aqueous solution interface. Isotherms are plotted from Eq. (121). In all plots, unless otherwise stated, $\varepsilon = 80$, $\varepsilon* = 5$, $\varepsilon_M = 2$, $\varkappa_{TF} = 2$ Å^{-1}, $a = 1$ Å, $c_b = 10$ mM, $\tilde{c} = 10$ mM, $W^* = -4k_BT$, $r_{\text{ads}} = 4$ Å, and $V_{\text{ads}} = 4\pi r_{\text{ads}}^3/3$. Note that the Debye length, κ^{-1} in all calculations here, accounts for both the bulk electrolyte and the adsorbing ion species concentrations. Panel (a) shows the effect of the adsorption radius, r_{ads}, effectively defining the density of the adsorption layer. Panel (b) shows the effect of varying the bulk concentration of specifically adsorbing ions, $\tilde{c}$. Panel (c) shows the shift of the isotherm with the TF screening length. Finally, panel (d) shows the isotherms plotted for different electrode materials, with parameters estimated as (i) Hg, $\varkappa_{TF} \approx 2$ Å^{-1}, $\varepsilon_M \approx 1.8$, with $\tilde{P}_0 = 0$ μC cm^{-2}; (ii) Au or Ag, $\varkappa_{TF} \approx 2$ Å^{-1}, $\varepsilon_M \approx 3$; (iii) Pt, $\varkappa_{TF} \approx 1.8$ Å^{-1}, $\varepsilon_M \approx 4$; and (iv) graphite, $\varkappa_{TF} \approx 0.28$ Å^{-1}, $\varepsilon_M \approx 12.5$, with $\tilde{P}_0 = 0$ μC cm^{-2}.

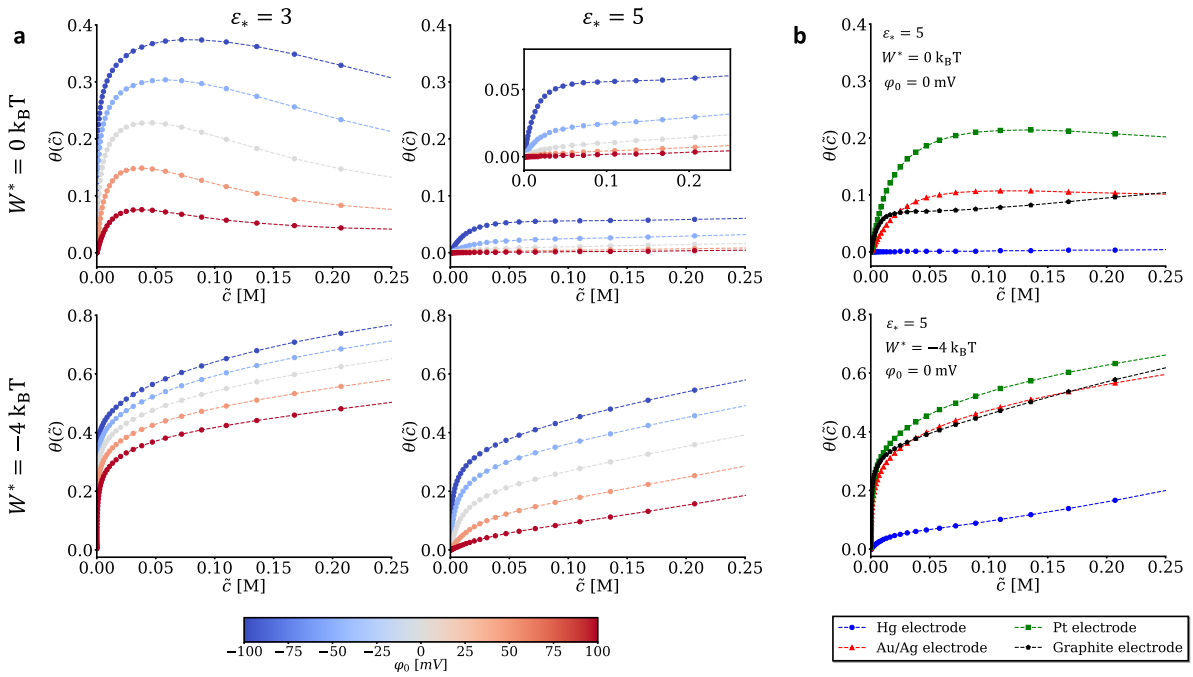

FIG. 11. Adsorption isotherms at the TF/nonlocal aqueous solution interface. Points for the adsorption isotherms were found by taking slices at a given electrode potential, φ_0, from calculations using Eq. (121) of the electrosorption isotherm $\theta(\varphi_0; \tilde{c})$ for different concentrations of adsorbing ions, $\tilde{c}$. Panel (a) shows how the adsorption isotherm varies with applied voltage φ_0 (−100 to +100 mV), short-range dielectric constant, ε_* (= 3, 5), and the specific interaction energy, W^* (= 0, $-4k_BT$). The inset for $\varepsilon_* = 5, W^* = 0k_BT$ (upper right) is the isotherms on an expanded y−axis. Other model parameters are taken to be $\varepsilon = 80$, $\varepsilon_M = 2$, $\varkappa_{TF} = 2$ Å^{-1}, $\tilde{P}_0 = 2$ μC cm^{-2}, $a = 1$ Å, $c_b = 10$ mM, $r_{ads} = 4$ Å, and $V_{ads} = 4\pi r_{ads}^3/3$. Panel (b) shows adsorption isotherms for different electrode materials at two values of the specific interaction energy, $W^* = 0k_BT$ (top) and $W^* = -4k_BT$ (bottom), with the corresponding TF parameters listed in Fig. 10. The Debye length, κ^{-1} in all calculations here, accounts for both the bulk electrolyte and the adsorbing ion species concentrations.

In Fig. 10(c), the TF length of the metal is varied. As the screening length gets larger ($\varkappa_{TF}$ decreases), the field of the charge is able to penetrate deeper into the metal, and so the repulsive branch of the self-energy is enhanced [see Fig. 8(b)], again leading to the requirement of higher negative voltages for adsorption. Of course, for different metals, it is not enough to merely adjust $\varkappa_{TF}$; the parameters ε_M, $\tilde{P}_0$, and W^* will also vary accordingly.

Regardless, it is interesting to see how different electrode materials may affect the isotherms within such a model. Here, we treat Hg, Au, Ag, Pt, and graphite electrodes. Of course, W^* will depend on these materials and also the nature of the ions, which are far from just being point charges. However, to explore the effect of other factors, we take W^* as constant across different materials but vary the parameters ε_M and $\varkappa_{TF}$, estimated from the electron densities and optical data on the plasmon frequency of the metals.[93] For Hg and graphite electrodes, it is also assumed that water dipoles lie parallel to the interface, i.e., $\tilde{P}_0 = 0$ μC cm^{-2}, whereas for Au, Ag, and Pt, we take $\tilde{P}_0 = 2$ μC cm^{-2}. Given the similar electron densities in Au and Ag, their parameters are taken to be the same for this study. Strictly, it is not possible to describe Pt and graphite well within the TF model, but we include results for the TF parameters that best represent these materials. For all materials, cation adsorption is, obviously, driven by more negative applied voltages. However, this adsorption is shown to be relatively easy for "good" metals, i.e., Pt, Au, and Ag, with these all showing non-zero coverages at positive applied voltages, reflecting the phenomenon of UPD. Despite the relatively large screening length in graphite, with $\varkappa_{TF}^{-1} \approx 3.6$ Å,[37] its high background permittivity pushes it to be comparable to these "good" metals. Hg, on the other hand, requires much more strongly negative applied voltages to reach similar coverages.

Adsorption isotherms: To explore this UPD phenomenon within the model further, it is instructive for us to obtain the concentration dependent adsorption isotherm, i.e., $\tilde{c}(\theta)$. This is, however, not as trivial to obtain as $\varphi_0(\theta)$ in Eq. (121). Given the inverse Debye length, κ, which will depend on both the concentration of the background electrolyte, c_b, and the concentration of the specifically adsorbing ions, $\tilde{c}$, a transcendental equation is obtained, coupling $\tilde{c}$ and θ. However, it is still possible to use Eq. (121) to find $\tilde{c}(\theta)$; by plotting the electrosorption isotherm for different values of $\tilde{c}$, as in Fig. 10(b), and taking slices along a constant φ_0, leading to the concentration dependent adsorption isotherm.

To determine if W^* or the self-energy profiles are responsible for UPD, we vary both W^* and ε_* within the model and plot the corresponding isotherms, $\theta(\tilde{c})$ in Fig. 11(a) for different surface potentials, φ_0. In all cases, increasing the bulk concentration of

adsorbing ions creates an entropic drive for ions to adsorb at the electrode. For positively charged adsorbing ions, a negative applied voltage strengthens this drive for adsorption, shifting the isotherm to greater coverages. This effect is sensitive to W_*. Naturally, by introducing some specific adsorption energy, there is a stronger drive for ions to adsorb at the interface; thus, the isotherms push to higher coverages, and the effect of UPD is more pronounced for $\varphi_0 > 0$ mV. However, this effect is also very sensitive to ε_*. As shown in Fig. 6(b), reducing ε_* to be more comparable with ε_M deepens the self-energy minimum. For $\varepsilon_* = 3$, the self-energy provides enough drive on its own to induce UPD, whereas for $\varepsilon_* = 5$, this effect is less pronounced. Of course, the exact value of ε_* is unknown, but it is supposedly somewhere between 3 and 5, leading the picture to be likely in between the two extremes shown here.

To explore this further, we plot the isotherms for different electrode materials held at $\varphi_0 = 0$ mV in Fig. 11(b), for $W^* = 0k_BT$ (top) and $W^* = -4k_BT$ (bottom). Even for $W^* = 0k_BT$ and $\varepsilon_* = 5$, the model predicts non-zero coverage across the concentration range for the "good" metals (Au, Ag, and Pt) and graphite. This result indicates that this self-energy minimum can indeed be an electrostatic impetus for UPD. For Hg, however, unless there is some favorable specific interaction energy, the isotherms predict that there will be no UPD.

It must be acknowledged that the developed theory does rest upon the mean field approximation, both in coupling the background electrolyte to the solvent structure and in these adsorption isotherms. Therefore, its validity rests upon comparison against experimental results.[94–96]

VII. CONCLUDING REMARKS

This paper revisited the classical electrostatic problem of a charge at the interface between two media, with a specific focus on the metal–solution electrochemical interface. We began by revisiting earlier approaches, such as the Specular Reflection Approximation (SRA), analyzing its results to understand the interplay between the dielectric properties of the two contacting media. While this method provided some useful insights, it had notable limitations, such as the inability to account for the overscreening dielectric response in the solution, leaving key physical phenomena unexplained. These challenges inspired the development of the current work: a more robust field-theoretical framework designed to model the interface between two nonlocal screening media, such as metals and aqueous electrolytes, free from oversimplified assumptions.

By constructing a free-energy functional and simplifying the system to include a Lorentzian solvent coupled with a Debye–Hückel medium, we derived the governing equations for both the metal and the solution. Using a Fourier–Bessel approach to solve for the electrostatic potential distribution and the self-energy of a point charge, we obtained significant insights into the behavior of charges at a sharp metal–solution boundary.

Our results aligned qualitatively with the SRA in predicting an adsorption minimum in the self-energy, hinting at a purely electrostatic mechanism that facilitates ion physisorption at the interface. This phenomenon is directly linked to the penetration of the electric field into the electrode. Moreover, incorporating the effects of interfacial water dipoles revealed asymmetries in the self-energy profiles for positive and negative ions. When water molecules orient their negative ends toward the electrode, a repulsive adsorption barrier can arise for positive ions, with its height strongly influenced by the system's parameters.

Our study also explored how an externally applied voltage affects the system, producing diverse adsorption behaviors that reflect the complex interplay of forces at the interface. While direct comparisons to experimental or simulation data remain limited at this stage, our approach offers qualitative predictions that are consistent with simulation studies of ion adsorption in aqueous electrolytes. Indeed, this model is still in its early stages of development and is based on a sharp interface approximation. As such, it lacks the level of detail necessary to directly connect experimental capacitance measurements with ion adsorption behaviors. Unlike some earlier models, which relied on fitting multiple unknown parameters to experimental data, this framework prioritizes theoretical clarity and flexibility for future improvements.

This paper, however, sets a baseline upon which we can extend and refine the model. For instance, the impact of ion size can be incorporated using approximations such as the Born sphere model, rather than the simple point charge approximation used here. The most promising direction, however, involves introducing the overscreening dielectric response of the solvent. By adopting a higher-order Landau–Ginzburg expansion, the model would predict oscillatory self-energy profiles for ions, uncovering finer details about the role of water structure in electrosorption. Of particular interest will be how the oscillatory potential distributions induced by both the surface and the ion will interfere with each other and how this will manifest in the overall structure of the electrical double layer.

The issue of accounting for overscreening in electrostatics at the metal/electrolyte interface does, however, remain a persistent challenge. When applying the SRA equations from Ref. 22 in conjunction with the approximation of water's nonlocal dielectric constant $\varepsilon(k)$, which includes divergence points associated with overscreening, the key integrals in these equations become divergent. This limitation motivated the development of this alternative field-theoretical approach, with the expectation that extending the free energy functional to higher-order gradients might resolve the issue. However, this approach has not yet yielded a solution, and the present analysis is restricted to first-order gradient terms. Nevertheless, the proposed framework in this paper (i) provides a foundation for future extensions that may address overscreening and (ii) enables the incorporation of specific surface effects through the introduction of surface polarization.

The overscreening effect is suppressed by nonlinear effects (see Ref. 97); however, in calculations of electrostatic potentials generated by charges in the bulk, it does not result in any divergence of the electric field.[98] This is because the diverging $\varepsilon(k)$ appears in the denominators, and in a pure solvent without an added electrolyte, those denominators do not cross zero (in the presence of electrolytes—Debye screening, additional techniques are required to address this issue[99]). However, divergences do arise in expressions describing the electric field of ions near the interface when $\varepsilon(k)$ becomes negative. However, from a physical perspective, no fundamental justification exists for expecting divergences due to the structure of water. Such divergences typically indicate a resonance phenomenon, but it is unclear what specific resonance would

arise from the interplay between the nonlocal dielectric response of water and the metal. While incorporating nonlinear effects may yield a more realistic description of the system, it does not inherently resolve the "divergence-problem."

While these advancements will inevitably add complexity, they hold the potential to unlock deeper insights into the mechanisms at play in electrochemical interfaces. By building on this foundation, we aim to bridge our theoretical predictions with both the results of experiments and simulations, with the goal of a more comprehensive understanding of these systems.

ACKNOWLEDGMENTS

J.G.H. acknowledges the support from the Imperial College President's PhD Scholarship and the Turing Scheme Global Fellowship. Both J.G.H. and A.A.K. acknowledge the support of the Leverhulme Trust under Grant No. RPG-2022-142. H.B. acknowledges CNRS for EMERGENCE@INC2023 funding.

AUTHOR DECLARATIONS

Conflict of Interest

The authors have no conflicts to disclose.

Author Contributions

Jonathan G. Hedley: Conceptualization (equal); Formal analysis (equal); Funding acquisition (equal); Investigation (equal); Methodology (equal); Project administration (equal); Visualization (equal); Writing – original draft (equal); Writing – review & editing (equal). **Kavin K. Bhatt**: Formal analysis (supporting); Investigation (supporting); Methodology (supporting). **Hélène Berthoumieux**: Formal analysis (equal); Investigation (equal); Methodology (equal); Supervision (supporting); Writing – review & editing (supporting). **Alexei A. Kornyshev**: Conceptualization (equal); Formal analysis (equal); Investigation (equal); Project administration (equal); Supervision (equal); Writing – original draft (equal); Writing – review & editing (equal).

DATA AVAILABILITY

Data sharing is not applicable to this article as no new data were created or analyzed in this study.

APPENDIX: COMPARATIVE ANALYSIS BETWEEN SPECULAR REFLECTION APPROXIMATION AND FIELD-THEORETICAL APPROACHES

Throughout this paper, we have presented a detailed analysis of the developed field-theoretical (FT) approach. However, for some brevity in the main text, these results were not directly compared against the results of the specular reflection approximation. Notably, the general expression for the electrostatic potential distribution at the interface derived in Ref. 22 and presented in Eqs. (11)–(13), while having been used extensively in the literature over the past 45 years, has never, to our knowledge, been numerically validated against the asymptotic laws presented in Table I. Thus, we provide in this appendix an additional detailed analysis of this method to add to the pedagogical nature of this paper, while also further showing how our FT method fits into the picture.

1. Thomas–Fermi metal/local water

Let us begin with the case of an interface between a Thomas–Fermi metal, with a dielectric function described by Eq. (16), and a local dielectric description of water, with a dielectric constant $\varepsilon = 80$. Using Eqs. (11)–(13) and the local approximation for the dielectric function of water, i.e., $\varepsilon_{\mathrm{I}}(k) \equiv \varepsilon$, the lateral electrostatic potential distribution (see Sec. V B) created by a point charge placed at a distance a from the interface can be derived within the SRA as

$$\frac{\varepsilon}{q} u_{\parallel,\mathrm{SRA}}(z = a, R; \gamma = 1) = \frac{1}{R} - \frac{1}{\sqrt{R^2 + 4a^2}} + 2\int_0^\infty dK\, J_0(KR) \times \left(\frac{\xi K}{\xi K + \sqrt{K^2 + \varkappa_{\mathrm{TF}}^2}}\right) e^{-2Ka}. \tag{A1}$$

Expressing Eq. (A1) in this form allows easy interpretation; the first term clearly relates to the Coulomb potential created by the ion in the bulk, the second term relates to the potential generated by the image of the charge, and the third is a correction term accounting for the imperfect screening of the metal. Note that in the case of a perfect metal, i.e., $\xi \to 0$, the correction term disappears, and Eq. (A1) becomes the classical expression for the electrostatic potential distribution at a conductor/dielectric interface.

For the same system, Eq. (107), i.e., the FT approach, reduces to be exactly equivalent to Eq. (A1). While showing that the FT and SRA formulations are equivalent in the case of local water is perhaps beneficial in validating our present approach, it is not a surprising result. In the local approximation, it is expected that the SRA should reproduce the exact result for this system. Therefore, it should coincide with the FT result.

We can perform some straightforward analyses of this result. Plotting Eq. (A1) in Fig. 12(a) against the limiting laws presented in Table I, we very readily see that this expression simply interpolates between the short (1) and long (3) distance laws. However, we see that these laws only apply in very extreme cases, i.e., very close to ($R < 1$ Å) or very far ($R > 100$ Å) from the charge.

2. Thomas–Fermi metal/nonlocal water

Perhaps the more interesting case to examine here is how the two approaches differ when a nonlocal medium is considered. Again, we consider here the simple case where surface polarization from chemisorbed water and applied voltages are neglected to allow a direct comparison between the SRA and FT approaches.

The result for the FT approach is already presented in Eq. (107) of the main text. Within the SRA, Eqs. (11)–(13) yield the lateral interaction potential for the TF metal/Lorentzian water interface as

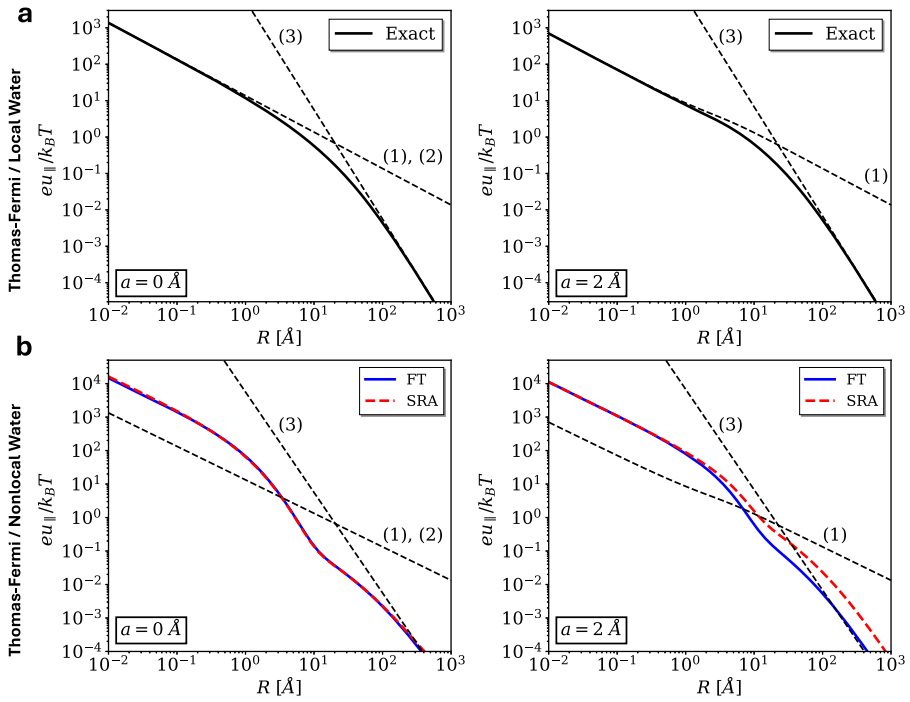

FIG. 12. Comparison of lateral electrostatic potential profiles between the field-theoretical (FT) and specular reflection approximation (SRA) approaches. (a) Log scale plots of Eq. (A1) against the limiting laws presented in Table I, for $a = 0$ Å (left) and $a = 2$ Å (right). Equation (A1) is equivalent to Eq. (A2), and so only one curve is plotted here for both FT and SRA. (b) Log scale plots of Eq. (107), the FT approach (blue) against Eq. (A3), and the SRA approach (red), for $a = 0$ Å (left) and $a = 2$ Å (right). Again, for comparison, the limiting laws presented in Table I are also plotted. For all plots, $\varepsilon = 80$, $\varepsilon_* = 5$, $\Lambda = 3$ Å, $\varepsilon_M = 2$, and $\varkappa_{TF} = 2$ Å^{-1}.

$$\frac{\varepsilon}{q}u_{\parallel,\mathrm{SRA}}(z=a,R) = \frac{1}{R}\left[1+(\gamma-1)e^{-R/\Lambda}\right] + \frac{1}{\sqrt{R^2+4a^2}}\left[1+(\gamma-1)e^{-\sqrt{R^2+4a^2}/\Lambda}\right] - 2\int_0^\infty dK\, J_0(KR) \times \frac{\left[e^{-Ka}+\frac{K(\gamma-1)}{\sqrt{K^2+1/\Lambda^2}}e^{-a\sqrt{K^2+1/\Lambda^2}}\right]^2}{1+\frac{K(\gamma-1)}{\sqrt{K^2+1/\Lambda^2}}+\frac{\xi K}{\sqrt{K^2+\varkappa_{TF}^2}}}. \quad \text{(A2)}$$

As above, we can make some direct analytical comparisons between the two approaches. Considering first the charge directly at the interface, i.e., at $a = 0$ Å, we can write for $\mathcal{U}_{\mathrm{pure}}$,

$$\mathcal{U}_{\mathrm{pure}}(K;a=0) = \frac{\xi K - \sqrt{K^2+\varkappa_{TF}^2}\left(1+\frac{K(\gamma-1)}{\sqrt{K^2+1/\Lambda^2}}\right)}{\xi K + \sqrt{K^2+\varkappa_{TF}^2}\left(1+\frac{K(\gamma-1)}{\sqrt{K^2+1/\Lambda^2}}\right)}. \quad \text{(A3)}$$

Inserting this into Eq. (107), we obtain

$$\frac{\varepsilon}{q}u_{\parallel,\mathrm{FT}}(R;a=0) = \frac{1}{R}\left[1+(\gamma-1)e^{-R/\Lambda}\right] + \int_0^\infty dK\, J_0(KR) \times \left(1+\frac{K(\gamma-1)}{\sqrt{K^2+1/\Lambda^2}} - \frac{2}{1+\frac{K(\gamma-1)}{\sqrt{K^2+1/\Lambda^2}}+\frac{\xi K}{\sqrt{K^2+\varkappa_{TF}^2}}} \times \left(1+\frac{K(\gamma-1)}{\sqrt{K^2+1/\Lambda^2}}\right)^2\right). \quad \text{(A4)}$$

Using that

$$\int_0^\infty dK\, J_0(KR)\left(1+\frac{K(\gamma-1)}{\sqrt{K^2+1/\Lambda^2}}\right) = \frac{1}{R}\left[1+(\gamma-1)e^{-R/\Lambda}\right], \quad \text{(A5)}$$

we find that $u_{\parallel,\mathrm{FT}}(R;\ a=0) = u_{\parallel,\mathrm{SRA}}(R;\ a=0)$. This is also verified through exact numerical calculations, plotted in Fig. 12(b) (left). This equivalence can be attributed to the SRA not coming into effect if the charge is sitting directly at the interface. Moving the charge just slightly away from the interface exemplifies this; consider now the charge sitting slightly away at $a = 2$ Å [Fig. 12(b) (right)]. Close to the charge ($R < 1$ Å), the potential is dominated by the Coulomb $1/R$ term, and so both approaches coincide. However, it can generally be seen that the lateral potential is overestimated at all distances within the SRA compared to the FT approach. This finding is beneficial for our picture of ion adsorption, as it indicates that charges experience a stronger reduction in the repulsive electrostatic potential than in the SRA model.

REFERENCES

[1] H. Helmholtz, "Ueber einige Gesetze der Vertheilung elektrischer Ströme in körperlichen Leitern mit Anwendung auf die thierisch-elektrischen Versuche," Ann. Phys. **165**, 211 (1853).
[2] H. Helmholtz, "Studien über electrische Grenzschichten," Ann. Phys. **243**, 337 (1879).
[3] M. G. Gouy, "Sur la constitution de la charge électrique à la surface d'un électrolyte," J. Phys. Théor. Appl. **9**, 457 (1910).
[4] D. L. Chapman, "LI. A contribution to the theory of electrocapillarity," Philos. Mag. **25**, 475 (1913).
[5] O. Stern, "Zur theorie der elektrolytischen doppelschicht," Z. Elektrochem. Angew. Phys. Chem. **30**, 508 (1924).

[6]M. R. Philpott and J. N. Glosli, "Screening of charged electrodes in aqueous electrolytes," J. Electrochem. Soc. **142**, L25 (1995).
[7]M. R. Philpott, J. N. Glosli, and S. B. Zhu, "Molecular dynamics simulation of adsorption in electric double layers," Surf. Sci. **335**, 422 (1995).
[8]E. Spohr, "Computer simulation of the structure of the electrochemical double layer," J. Electroanal. Chem. **450**, 327 (1998).
[9]E. Spohr, "Molecular simulation of the electrochemical double layer," Electrochim. Acta **44**, 1697 (1999).
[10]D. I. Dimitrov and N. D. Raev, "Molecular dynamics simulations of the electrical double layer at the 1 M KCl solution|Hg electrode interface," J. Electroanal. Chem. **486**, 1 (2000).
[11]A. Limaye, D. Suvlu, and A. P. Willard, "Water molecules mute the dependence of the double-layer potential profile on ionic strength," Faraday Discuss. **249**, 267 (2024).
[12]A. A. Kornyshev, E. Spohr, and M. A. Vorotyntsev, "Electrochemical interfaces: At the border line," in *Encyclopedia of Electrochemistry*, edited by A. J. Bard, M. Stratmann, E. Gileadi, and M. Urbakh (Wiley VCH, 2002), Vol. 1, pp. 33–132.
[13]M. Becker, P. Loche, M. Rezaei, A. Wolde-Kidan, Y. Uematsu, R. R. Netz, and D. J. Bonthuis, "Multiscale modeling of aqueous electric double layers," Chem. Rev. **124**, 1 (2024).
[14]J. G. Hedley, H. Berthoumieux, and A. A. Kornyshev, "The dramatic effect of water structure on hydration forces and the electrical double layer," J. Phys. Chem. C **127**, 8429 (2023).
[15]X. R. Advincula, E. H. G. Backus, M. Bonn, S. J. Cox, U. Diebold, A. Fellows, A. R. Finney, G. Goel, J. Hedley, Y. Jiang, D. Jin, V. Kapil, N. Kavokine, J. Klein, D. Laage, N. Mohandas, K. Morgenstern, T. Mukherjee, M. Olvera de la Cruz, H. Orlikowska-Rzeznik, S. Perkin, P. M. Piaggi, C. G. Rodellar, P. Ryan, T. Sayer, M. Seyffertitz, M. Shepelenko, G. C. Sosso, M. Thämer, A. Vilangottunjalil, R. Walker-Gibbons, Y. Wang, A. P. Willard, and P. Zhang, "Electrified/charged aqueous interfaces: General discussion," Faraday Discuss. **249**, 381 (2024).
[16]D. Martin-Jimenez, E. Chacon, P. Tarazona, and R. Garcia, "Atomically resolved three-dimensional structures of electrolyte aqueous solutions near a solid surface," Nat. Commun. **7**, 12164 (2016).
[17]T. Fukuma, Y. Ueda, S. Yoshioka, and H. Asakawa, "Atomic-scale distribution of water molecules at the mica-water interface visualized by three-dimensional scanning force microscopy," Phys. Rev. Lett. **104**, 016101 (2010).
[18]E. Nakouzi, S. Kerisit, B. A. Legg, S. Yadav, D. Li, A. G. Stack, C. J. Mundy, J. Chun, G. K. Schenter, and J. J. De Yoreo, "Solution structure and hydration forces between mica and hydrophilic versus hydrophobic surfaces," J. Phys. Chem. C **127**, 2741 (2023).
[19]A. Klaassen, F. Liu, F. Mugele, and I. Siretanu, "Correlation between electrostatic and hydration forces on silica and gibbsite surfaces: An atomic force microscopy study," Langmuir **38**, 914 (2022).
[20]S. Benaglia, H. Read, and L. Fumagalli, "Atomic-scale structure of interfacial water on gel and liquid phase lipid membranes," Faraday Discuss. **249**, 453 (2024).
[21]A. A. Kornyshev, A. I. Rubinshtein, and M. A. Vorotyntsev, "Image potential near a dielectric–plasma-like medium interface," Phys. Status Solidi B **84**, 125 (1977).
[22]M. A. Vorotyntsev and A. A. Kornyshev, "Electrostatic interaction on a metal-insulator interface," J. Exp. Theor. Phys. **51**, 509 (1980).
[23]A. I. Rubinshtein, "Image forces at the metal electrode-electrolyte solution interface: Account of spatial dispersion of the solution permittivity," Phys. Status Solidi B **120**, 65 (1983).
[24]J. Jackson, *Classical Electrodynamics*, 3rd ed. (Wiley, New York, NY, 1999).
[25]This wavenumber-dependent $\varepsilon(\mathbf{k})$ exists as such if $\varepsilon(\mathbf{r}, \mathbf{r}') = \varepsilon(\mathbf{r} - \mathbf{r}')$, which can be applicable to interfaces only under some crude approximations relating $\varepsilon(\mathbf{r}, \mathbf{r}')$ and $\varepsilon(\mathbf{r} - \mathbf{r}')$.
[26]J. C. Inkson, "The electrostatic image potential in metal semiconductor junctions," J. Phys. C: Solid State Phys. **4**, 591 (1971).
[27]A. A. Kornyshev and M. A. Vorotyntsev, "Nonlocal electrostatic approach to the double layer and adsorption at the electrode-electrolyte interface," Surf. Sci. **101**, 23 (1980).
[28]K. L. Kliewer and R. Fuchs, "Theory of dynamical properties of dielectric surfaces," in *Advances in Chemical Physics*, edited by I. Prigogine and S. A. Rice (John Wiley and Sons, New York, 1974), pp. 355–541.
[29]A. M. Gabovich, L. G. Il'Chenko, E. A. Pashitskii, and Y. A. Romanov, "Electrostatic energy and screened charge interaction near the surface of metals with different Fermi surface shape," Surf. Sci. Lett. **94**, A133 (1980).
[30]L. G. Il'Chenko, E. A. Pashitskii, and Y. A. Romanov, "Charge interaction in layered systems with spatial dispersion," Surf. Sci. Lett. **121**, 375 (1982).
[31]A. M. Gabovich, L. G. Il'Chenko, and E. A. Pashitskii, "Image forces and electron spectrum at the surface of liquid helium," Surf. Sci. **130**, 373 (1983).
[32]A. M. Gabovich, V. M. Rosenbaum, and A. I. Voitenko, "Dynamical image forces in three-layer systems and field emission," Surf. Sci. Lett. **186**, 294 (1987).
[33]A. M. Gabovich, Y. A. Reznikov, and A. I. Voitenko, "Excess nonspecific Coulomb ion adsorption at the metal electrode/electrolyte solution interface: Role of the surface layer," Phys. Rev. E **73**, 021606 (2006).
[34]A. M. Gabovich, V. M. Gun'ko, V. E. Klymenko, and A. I. Voitenko, "Role of dipole image forces in molecular adsorption," Eur. Phys. J. B **85**, 284 (2012).
[35]D. Horinek and R. R. Netz, "Specific ion adsorption at hydrophobic solid surfaces," Phys. Rev. Lett. **99**, 226104 (2007).
[36]L. Scalfi, T. Dufils, K. G. Reeves, B. Rotenberg, and M. Salanne, "A semiclassical Thomas–Fermi model to tune the metallicity of electrodes in molecular simulations," J. Chem. Phys. **153**, 174704 (2020).
[37]L. Scalfi and B. Rotenberg, "Microscopic origin of the effect of substrate metallicity on interfacial free energies," Proc. Natl. Acad. Sci. U. S. A. **118**, e2108769118 (2021).
[38]L. Scalfi, M. Salanne, and B. Rotenberg, "Molecular simulation of electrode-solution interfaces," Annu. Rev. Phys. Chem. **72**, 189 (2021).
[39]A. Schlaich, D. Jin, L. Bocquet, and B. Coasne, "Electronic screening using a virtual Thomas–Fermi fluid for predicting wetting and phase transitions of ionic liquids at metal surfaces," Nat. Mater. **21**, 237 (2022).
[40]A. T. Bui, F. L. Thiemann, A. Michaelides, and S. J. Cox, "Classical quantum friction at water–carbon interfaces," Nano Lett. **23**, 580 (2023).
[41]L. Joly, R. H. Meißner, M. Iannuzzi, and G. Tocci, "Osmotic transport at the aqueous graphene and hBN interfaces: Scaling laws from a unified, first-principles description," ACS Nano **15**, 15249 (2021).
[42]K. D. Fong, B. Sumić, N. O'Neill, C. Schran, C. P. Grey, and A. Michaelides, "The interplay of solvation and polarization effects on ion pairing in nanoconfined electrolytes," Nano Lett. **24**, 5024 (2024).
[43]N. Kavokine, M.-L. Bocquet, and L. Bocquet, "Fluctuation-induced quantum friction in nanoscale water flows," Nature **602**, 84 (2022).
[44]N. Kavokine, P. Robin, and L. Bocquet, "Interaction confinement and electronic screening in two-dimensional nanofluidic channels," J. Chem. Phys. **157**, 114703 (2022).
[45]A. Robert, H. Berthoumieux, and M.-L. Bocquet, "Coupled interactions at the ionic graphene-water interface," Phys. Rev. Lett. **130**, 076201 (2023).
[46]A. A. Kornyshev, "Nonlocal screening of ions in a structurized polar solvent: New aspects of solvent description in electrolyte theory," Electrochim. Acta **26**, 1 (1981).
[47]A. A. Kornyshev and W. Schmickler, "On the coverage dependence of the partial charge transfer coefficient," J. Electroanal. Chem. Interfacial Electrochem. **202**, 1 (1986).
[48]L. D. Landau and E. M. Lifshitz, *Electrodynamics of Continuous Media*, 2nd ed. (Pergamon Press, England, 1984).
[49]A. A. Kornyshev, "Nonlocal electrostatics of solvation," in *The Chemical Physics of Solvation*, edited by R. R. Dogonadze, E. Kalman, A. A. Kornyshev, and J. Ulstrup (Elsevier, 1985), Vol. A, pp. 77–118.
[50]P. A. Bopp, A. A. Kornyshev, and G. Sutmann, "Static nonlocal dielectric function of liquid water," Phys. Rev. Lett. **76**, 1280 (1996).
[51]P. A. Bopp, A. A. Kornyshev, and G. Sutmann, "Frequency and wave-vector dependent dielectric function of water: Collective modes and relaxation spectra," J. Chem. Phys. **109**, 1939 (1998).
[52]N. W. Ashcroft and N. D. Mermin, *Solid State Physics* (Harcourt Inc., 1976).
[53]A. Hildebrandt, R. Blossey, S. Rjasanow, O. Kohlbacher, and H.-P. Lenhof, "Novel formulation of nonlocal electrostatics," Phys. Rev. Lett. **93**, 108104 (2004).
[54]G. Monet, F. Bresme, A. A. Kornyshev, and H. Berthoumieux, "Nonlocal dielectric response of water in nanoconfinement," Phys. Rev. Lett. **126**, 216001 (2021).

[55]J. P. de Souza, A. A. Kornyshev, and M. Z. Bazant, "Polar liquids at charged interfaces: A dipolar shell theory," J. Chem. Phys. **156**, 244705 (2022).
[56]R. Blossey and R. Podgornik, "Continuum theories of structured dielectrics," Europhys. Lett. **139**, 27002 (2022).
[57]R. Blossey and R. Podgornik, "Field theory of structured liquid dielectrics," Phys. Rev. Res. **4**, 023033 (2022).
[58]R. Blossey and R. Podgornik, "A comprehensive continuum theory of structured liquids," J. Phys. A: Math. Theor. **56**, 025002 (2023).
[59]A. C. Maggs and R. Everaers, "Simulating nanoscale dielectric response," Phys. Rev. Lett. **96**, 230603 (2006).
[60]H. Berthoumieux and A. C. Maggs, "Fluctuation-induced forces governed by the dielectric properties of water—A contribution to the hydrophobic interaction," J. Chem. Phys. **143**, 104501 (2015).
[61]M. Vatin, A. Porro, N. Sator, J.-F. Dufrêche, and H. Berthoumieux, "Electrostatic interactions in water: A nonlocal electrostatic approach," Mol. Phys. **119**, e1825849 (2020).
[62]A. A. Kornyshev, "On the non-local electrostatic theory of hydration force," J. Electroanal. Chem. Interfacial Electrochem. **204**, 79 (1986).
[63]S. Marčelja and N. Radić, "Repulsion of interfaces due to boundary water," Chem. Phys. Lett. **42**, 129 (1976).
[64]K. Binder and P. C. Hohenberg, "Phase transitions and static spin correlations in Ising models with free surfaces," Phys. Rev. B **6**, 3461 (1972).
[65]M. I. Kaganov and A. N. Omel'Yanchuck, "Phenomenological theory of phase transition in a thin ferromagnetic plate," J. Exp. Theor. Phys. **34**, 895 (1972).
[66]R. Lipowsky and W. Speth, "Semi-infinite systems with first-order bulk transitions," Phys. Rev. B **28**, 3983 (1983).
[67]A. A. Kornyshev and S. Leikin, "Fluctuation theory of hydration forces: The dramatic effects of inhomogeneous boundary conditions," Phys. Rev. A **40**, 6431 (1989).
[68]F. Paillusson and R. Blossey, "Slits, plates, and Poisson-Boltzmann theory in a local formulation of nonlocal electrostatics," Phys. Rev. E **82**, 052501 (2010).
[69]H. Berthoumieux, "Gaussian field model for polar fluids as a function of density and polarization: Toward a model for water," J. Chem. Phys. **148**, 104504 (2018).
[70]M. R. Becker, P. Loche, D. J. Bonthuis, D. Mouhanna, R. R. Netz, and H. Berthoumieux, "Dielectric properties of aqueous electrolytes at the nanoscale," arXiv:2303.14846 [cond-mat.soft] (2023).
[71]R. Kjellander, "The intimate relationship between the dielectric response and the decay of intermolecular correlations and surface forces in electrolytes," Soft Matter **15**, 5866 (2019).
[72]R. Kjellander, "Nonlocal electrostatics in ionic liquids: The key to an understanding of the screening decay length and screened interactions," J. Chem. Phys. **145**, 124503 (2016).
[73]L. M. Varela, M. Perez-Rodriguez, M. Garcia, F. Sarmiento, and V. Mosquera, "Static structure of electrolyte systems and the linear response function on the basis of a dressed-ion theory," J. Chem. Phys. **109**, 1930 (1998).
[74]Y. A. Budkov, "Statistical field theory of ion–molecular solutions," Phys. Chem. Chem. Phys. **22**, 14756 (2020).
[75]A. A. Kornyshev, "Non-local dielectric response of a polar solvent and Debye screening in ionic solution," J. Chem. Soc., Faraday Trans. 2 **79**, 651 (1983).
[76]V. Kaiser, J. Comtet, A. Niguès, A. Siria, B. Coasne, and L. Bocquet, "Electrostatic interactions between ions near Thomas–Fermi substrates and the surface energy of ionic crystals at imperfect metals," Faraday Discuss. **199**, 129 (2017).
[77]S. Nair, G. Pireddu, and B. Rotenberg, "Induced charges in a Thomas-Fermi metal: Insights from molecular simulations," Mol. Phys. (published online 2024).
[78]M. L. Belaya, V. G. Levadny, and D. A. Pink, "Electric double layer near soft permeable interfaces. 1. Local electrostatic," Langmuir **10**, 2010 (1994).
[79]M. L. Belaya, V. G. Levadny, and D. A. Pink, "Electric double layer near soft permeable interfaces. 2. "Nonlocal" theory," Langmuir **10**, 2015 (1994).
[80]R. Parsons and F. G. R. Zobel, "The interphase between mercury and aqueous sodium dihydrogen phosphate," J. Electroanal. Chem. **9**, 333 (1965).
[81]A. A. Kornyshev, W. Schmickler, and M. A. Vorotyntsev, "Nonlocal electrostatic approach to the problem of a double layer at a metal-electrolyte interface," Phys. Rev. B **25**, 5244 (1982).
[82]O. A. Petrii and G. A. Tsirlina, "Electrode potentials," in *Encyclopedia of Electrochemistry*, edited by A. J. Bard *et al.* (Wiley VCH, 2002), Vol. 1, pp. 33–132.
[83]K. Ojha, K. Doblhoff-Dier, and M. T. M. Koper, "Double-layer structure of the Pt(111)–aqueous electrolyte interface," Proc. Natl. Acad. Sci. U. S. A. **119**, e2116016119 (2022).
[84]O. K. Rice, "Application of the Fermi statistics to the distribution of electrons under fields in metals and the theory of electrocapillarity," Phys. Rev. **31**, 1051 (1928).
[85]N. F. Mott and R. J. Watts-Tobin, "The interface between a metal and an electrolyte," Electrochim. Acta **4**, 79 (1961).
[86]A. A. Kornyshev and M. A. Vorotyntsev, "Field-induced interfacial relaxation and electrical properties of the compact layer," J. Electroanal. Chem. Interfacial Electrochem. **167**, 1 (1984).
[87]A. A. Kornyshev, "Metal electrons in the double layer theory," Electrochim. Acta **34**, 1829 (1989).
[88]M. A. Vorotyntsev and S. N. Ivanov, "Statistical-mechanics of an ion ensemble adsorbed on a metal-dielectric interface," J. Exp. Theor. Phys. **88**, 1729 (1985).
[89]M. A. Vorotyntsev, A. A. Kornyshev, and A. I. Rubinshtein, "Electrostatic interaction of ions in solution on the electrode surface: The effects of ion-field penetration in the electrode," Dokl. Akad. Nauk SSSR **248**, 1321 (1979).
[90]A. J. Bard and L. R. Faulkner, *Electrochemical Methods, Fundamentals and Applications* (John Wiley and Sons, 1980).
[91]V. S. Bagotsky, *Fundamentals of Electrochemistry* (John Wiley and Sons, 2005).
[92]E. Herrero, L. J. Buller, and H. D. Abruna, "Underpotential deposition at single crystal surfaces of Au, Pt, Ag and other materials," Chem. Rev. **101**, 1897 (2001).
[93]M. A. Vorotyntsev and A. A. Kornyshev, "See table 1 in: Models to describe collective properties of the metal/solvent interface in electric double-layer theory," Sov. Electrochem. **20**, 1 (1984).
[94]M. A. Vorotyntsev, "Modern state of double layer study of solid metals," in *Modern Aspects of Electrochemistry*, edited by J. M. Bokris, B. E. Conway, and R. E. White (Springer, 1986), Vol. 17, pp. 131–222.
[95]W. Schmickler, "Adsorption on metal electrodes," in *Interfacial Electrochemistry* (Oxford Academic, 1996).
[96]W. Schmickler and E. Santos, *Interfacial Electrochemistry* (Springer, 2010).
[97]M. V. Fedorov and A. A. Kornyshev, "Unravelling the solvent response to neutral and charged solutes," Mol. Phys. **105**, 1 (2007).
[98]A. A. Kornyshev and G. Sutmann, "The shape of the nonlocal dielectric function of polar liquids and the implications for thermodynamic properties of electrolytes: A comparative study," J. Chem. Phys. **104**, 1524 (1996).
[99]A. Levy, M. Bazant, and A. A. Kornyshev, "Ionic activity in concentrated electrolytes: Solvent structure effect revisited," Chem. Phys. Lett. **738**, 136915 (2020).